Interaction Notes

Note 215

July 1974

Excitation of a Terminated TEM Transmission Line Through a Small Aperture

Darko Kajfez
University of Mississippi
University, Mississippi 38677

Abstract

The coupling of the energy from an incident plane wave to a transmission line situated behind a plane screen is computed by the use of equivalent electric and magnetic dipole moments. The frequency and time responses of the voltage at the transmission-line terminals are evaluated from the equivalent circuit consisting of one voltage generator and one current generator. It was found that the circular hole and a single-wire transmission line have directional property when a TM incident wave is arriving in parallel with the screen surface.

This study was performed under subcontract to

The Dikewood Corporation
1009 Bradbury Drive, S.E.
University Research Park
Albuquerque, New Mexico 87106

and has been fully supported by the Defense Nuclear Agency (DNA) under

DNA Subtask EB088
EMP Interaction and Coupling
DNA Work Units 32 and 33
Coupling Characteristics of Apertures
Coaxial Cables

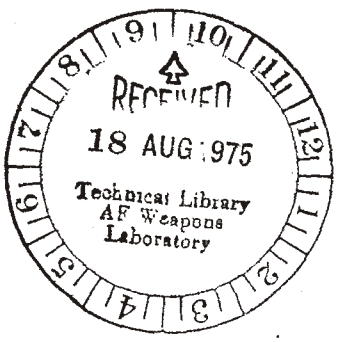

CONTENTS

ILLUSTRATIONS

ILLUSTRATIONS (Continued)

SECTION I

Introduction

The general problem addressed in this study is how does electromagnetic energy incident upon an infinite ground screen containing an aperture couple to wire transmission lines residing behind the screen. In this initial investigation discussion is restricted to the simple case shown in Figure 1-1. of a single z-directed line of infinite extent behind a screen containing an aperture which is dimensionally vanishingly small. The solution may serve as a Green's function for more general aperture shapes.

Several simplifying assumptions are made. First, the quantity of interest is taken to be the energy propagated away from the aperture on the line and not local, evanescent phenomena. This obviates a detailed investigation of the more difficult aperture region of the line. Second, the primary carrier of energy is assumed to be the TEM mode, and any higher order modes are ignored. The analysis is first-order and serves as a base for more exact investigation. Such representation of the electromagnetic field on a transmission line in terms of the TEM wave is discussed in detail in Interaction Note 148, ref. [1].

For purposes of computation of the fields inside the screen, the aperture is replaced with some equivalent source distribution residing on the surface of an infinite, unbroken ground screen. Allowance is made for either a magnetic surface current analog or a dipole moment equivalent in which both electric and magnetic sources may be present. These sources can be computed from the aperture fields which are the solution of the boundary value problem for the given aperture. At present, we assume that the solution for the given aperture has been found, and that the equivalent electric and magnetic dipole moments $\vec{p}_a$ and $\vec{m}_a$ are computed from this solution. The methods of computation of dipole moments have

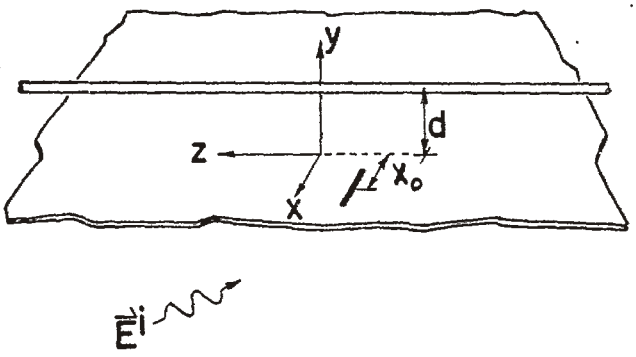

Fig. 1-1. System to be investigated.

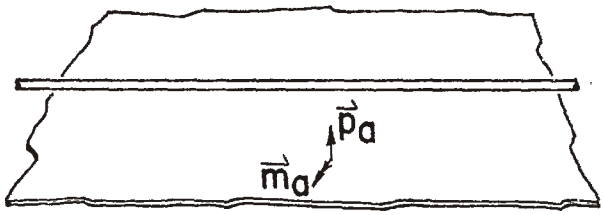

Fig. 1-2. Aperture replaced by electric dipole moment $\vec{p}_a$ and magnetic dipole moment $\vec{m}_a$.

been discussed in the Interaction Note 132, ref. [2], and in the Sensor and Simulation Note 125, ref [3]. It is appropriate to mention here an important difference in notation between these two notes and the present report.

In the present report, the electric dipole moment p_a (in Ampere•meters) denotes the moment of the electric current element, much in the same way as in references [4], [5], and [6]. The above mentioned references [2] and [3] are using the moment of the electric charge doublet p (in Coulomb•meters). The relationship between the two notations is

$$p_a = j\omega p \quad . \tag{1-1}$$

Similarly, the magnetic dipole moment m_a (in Volt•meters) used here represents the moment of the magnetic current element, in agreement with references [7], [8], and [9]. The relationship between m_a and m defined in [3] is, for circular aperture,

$$m_a = -j\omega\mu m \quad . \tag{1-2}$$

Given the simple sources of Figure 1-2., one may readily draw the equivalent circuit for the excitation of the transmission line, shown in Figure 1-3., where the ideal current source ΔI is related linearly to the magnitude p_a of the electric dipole moment and where the ideal voltage source ΔV is similarly related to the magnitude m_a of the magnetic dipole moment.

The equivalent circuit in Figure 1-3 is of great value for computing the terminal voltages V_3 and V_4 on the transmission line for any particular incident waveforms. The frequency-domain response of V_3 and V_4 is discussed in Section 3 of this report, while the time-domain response is discussed in Section 4. Several examples have been worked out, and the resulting waveforms are shown in that Section.

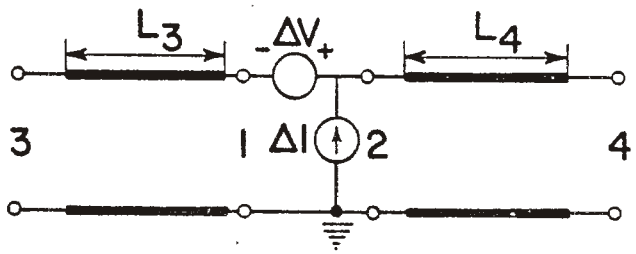

Fig. 1-3. Simple equivalent circuit for the transmission line.

The derivation of the background formulas is organized in four Appendices. Appendix A summarizes the TEM field configuration on the single wire above a ground plane. The coupling coefficients have been derived in two different ways in Appendices B and C. Appendix D explains why a small aperture can be replaced by a pair of dipoles. Also, Appendix D demonstrates the presence of the quadrupole term $\partial H_{bx}/dx$, which is neglected in the dipole representation.

SECTION II

Problem Description

The coupling of the electromagnetic field through an aperture to the single-wire transmission line is illustrated in Fig. 2-1. A circular aperture of radius a is centered at the point $(x_o, 0, 0)$. A circular wire of radius r is situated at height d above the perfectly conducting ground plane of infinite extent. The wire lengths in each direction from the aperture are denoted by ℓ_3 and ℓ_4. At these ends there may be attached some lumped resistances. The problem to be solved in this report is to compute the voltages V_3 and V_4 at each end of the single-wire transmission line for a known electromagnetic wave incident from below the ground plane.

There are two basic orientations of the incident plane wave: transverse electric (TE) and transverse magnetic (TM) wave, as shown in Fig. 2-1. TE wave is oriented so that the $\vec{E}$ vector is parallel with the ground plane, while in TM wave the vector $\vec{H}$ is parallel with the ground plane. The plane of incidence is specified by angle α and the angle of incidence by angle θ. Vector $\vec{k}$ is pointing in the direction of propagation and has its magnitude equal to the free-space propagation constant k for real, positive ω.

In an incident plane wave, the magnitudes of electric and magnetic fields are related through the intrinsic impedance η as follows

$$E_o^i = H_o^i \eta \qquad (2\text{-}1)$$

The components of interest for the coupling through the aperture are the normal electric and the tangential magnetic fields, which are:

TM: $$E_n^i = E_o \sin\theta \quad , \quad H_t^i = H_o \quad , \qquad (2\text{-}2)$$

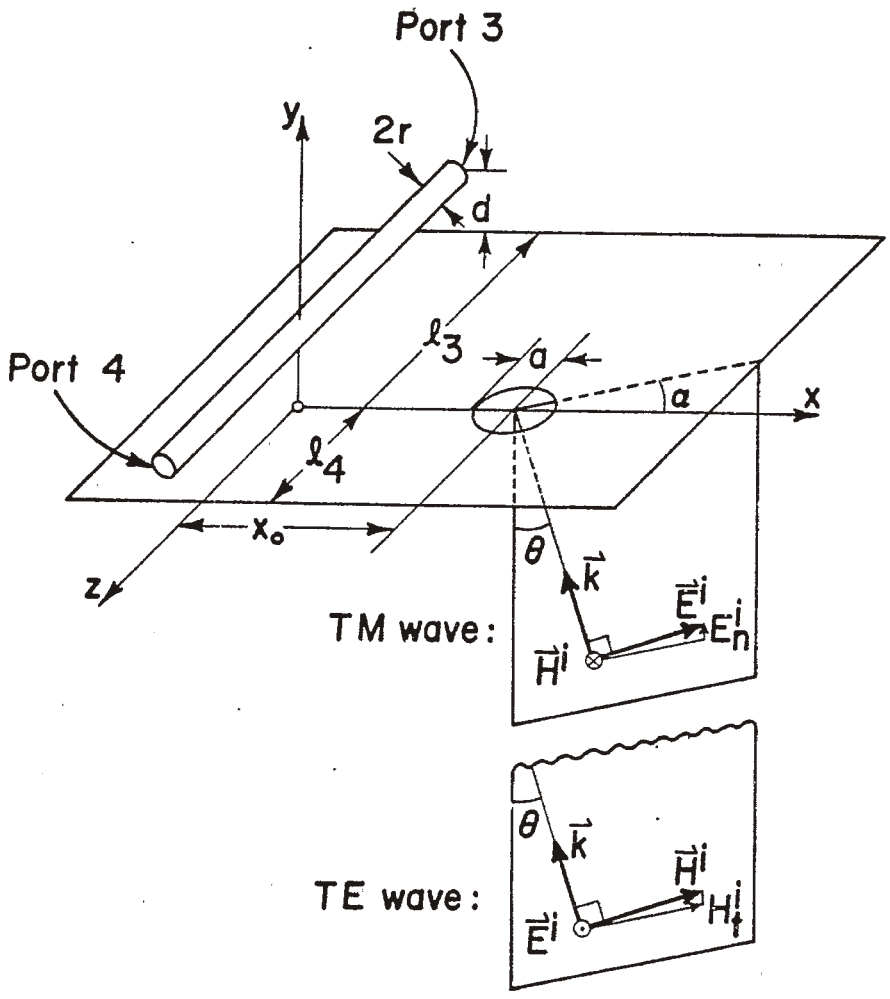

Fig. 2-1. The geometry of the problem to be investigated.

$$\underline{\text{TE}}: \quad E_n^i = 0 \quad , \quad H_t^i = H_o \cos\theta \quad . \tag{2-3}$$

The x and y components of these fields are:

$$\underline{\text{TM}}: \quad E_y^i = E_o \sin\theta \quad , \quad H_x^i = -H_o \sin\alpha \quad , \tag{2-4}$$

$$\underline{\text{TE}}: \quad E_y^i = 0 \quad , \quad H_x^i = H_o \cos\Theta \cos\alpha \quad . \tag{2-5}$$

On the surface of a perfect conductor, the total normal electric and tangential magnetic fields are double the corresponding incident field components:

$$\underline{\text{TM}}: \quad E_y^{tot} = 2E_o \sin\theta \quad , \quad H_x^{tot} = -\frac{2E_o}{\eta}\sin\alpha \quad , \tag{2-6}$$

$$\underline{\text{TE}}: \quad E_y^{tot} = 0 \quad , \quad H_x^{tot} = \frac{2E_o}{\eta}\cos\theta\cos\alpha \quad . \tag{2-7}$$

SECTION III

Response in the Frequency Domain

The excitation of a single-wire transmission line through a small aperture is modeled by the circuit in Fig. 3-1. Generators ΔI and ΔV represent the aperture electric and magnetic dipoles, located at z=0. The twoports 1-3 and 2-4 represent the transmission line sections of lengths ℓ_3 and ℓ_4. The resistances R_3 and R_4 are the external terminations. Assuming that the functions $\Delta V(\omega)$ and $\Delta I(\omega)$ are known, the terminal voltages $V_3(\omega)$ and $V_4(\omega)$ will be computed.

From Kirchhoff laws it follows

$$\Delta I = I_1 + I_2 \quad , \tag{3-1}$$

$$\Delta V = V_2 - V_1 \quad . \tag{3-2}$$

The circuit will be solved by the use of scattering parameters. First, the currents and voltages at each of the ports i=1 through 4 will be separated in the incident (superscript +) and outgoing (superscript -) parts:

$$V_i = V_i^+ + V_i^- \quad ; \quad I_i = \frac{1}{Z_o}(V_i^+ - V_i^-) \quad , \tag{3-3}$$

where Z_o is the characteristic impedance. Next, the normalized scattering parameters a and b will be introduced:

$$a_i = \frac{V_i^+}{\sqrt{Z_o}} \quad ; \quad b_i = \frac{V_i^-}{\sqrt{Z_o}} \quad . \tag{3-4}$$

In terms of scattering parameters, (3-1) and (3-2) become

$$\Delta I = \frac{1}{\sqrt{Z_o}} (a_1 + a_2 - b_1 - b_2) \quad , \tag{3-5}$$

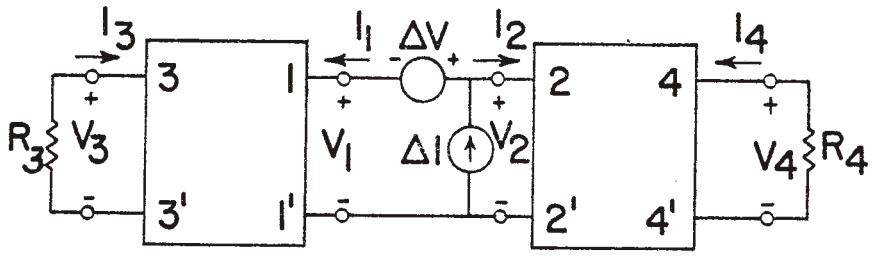

Fig. 3-1. Equivalent twoport circuit for the transmission line.

$$\Delta V = \sqrt{Z_o}\,(-a_1 + a_2 - b_1 + b_2) \quad . \tag{3-6}$$

This can be rearranged as

$$a_1 = \frac{1}{2}\left(\Delta I\,\sqrt{Z_o} - \frac{\Delta V}{\sqrt{Z_o}}\right) + b_2 \quad , \tag{3-7}$$

$$a_2 = \frac{1}{2}\left(\Delta I\,\sqrt{Z_o} + \frac{\Delta V}{\sqrt{Z_o}}\right) + b_1 \quad . \tag{3-8}$$

For simple sections of transmission line, the scattering matrices are given by

$$\begin{pmatrix} b_2 \\ b_4 \end{pmatrix} = e^{-jk\ell_4} \begin{pmatrix} 0 & 1 \\ 1 & 0 \end{pmatrix} \begin{pmatrix} a_2 \\ a_4 \end{pmatrix} \tag{3-9}$$

for the right-hand section, and

$$\begin{pmatrix} b_1 \\ b_3 \end{pmatrix} = e^{-jk\ell_3} \begin{pmatrix} 0 & 1 \\ 1 & 0 \end{pmatrix} \begin{pmatrix} a_1 \\ a_3 \end{pmatrix} \tag{3-10}$$

for the left-hand section.
Furthermore, the terminations R_3 and R_4 produce reflection coefficients ρ_3 and ρ_4 as follows

$$\rho_3 = \frac{a_3}{b_3} = \frac{R_3 - Z_o}{R_3 + Z_o} \quad , \tag{3-11}$$

$$\rho_4 = \frac{a_4}{b_4} = \frac{R_4 - Z_o}{R_4 + Z_o} \tag{3-12}$$

(3-7) through (3-12) contain 8 linear equations relating 8 unknown coefficients a_i and b_i. The system may be solved by

simple eliminations. The two scattering coefficients of interest are b_3 and b_4:

$$b_3 = \frac{1}{2} \cdot \frac{P\rho_4 e^{-jk\ell_4} + Me^{jk\ell_4}}{e^{jk\ell_{tot}} - \rho_3\rho_4 e^{-jk\ell_{tot}}} \tag{3-13}$$

$$b_4 = \frac{1}{2} \cdot \frac{M\rho_3 e^{-jk\ell_3} + Pe^{jk\ell_3}}{e^{jk\ell_{tot}} - \rho_3\rho_4 e^{-jk\ell_{tot}}} \tag{3-14}$$

where $\ell_{tot} = \ell_3 + \ell_4$, and

$$P = \Delta I \sqrt{Z_o} + \frac{\Delta V}{\sqrt{Z_o}} \quad , \quad M = \Delta I \sqrt{Z_o} - \frac{\Delta V}{\sqrt{Z_o}} \quad . \tag{3-15}$$

The voltages at ports 3 and 4 can be obtained from the scattering coefficients b_3 and b_4 in the following way:

$$V_3 = \sqrt{Z_o}\ (1 + \rho_3) b_3 \quad , \tag{3-16}$$

$$V_4 = \sqrt{Z_o}\ (1 + \rho_4) b_4 \quad . \tag{3-17}$$

Therefore, the problem has been solved. Output voltages are expressed terms of sources ΔI and ΔV. In Appendix C, ΔI and ΔV have been expressed in terms of aperture moments p_a and m_a. For a small aperture of an arbitrary shape, the moments can be computed by integrating the aperture field distribution as explained in Appendix D. This field must be obtained from a solution of the boundary value problem for a particular aperture.

A special case of a small circular aperture will be investigated next, since there are simple analytic expressions available for its dipole moments. The case of the TM incident wave will be selected as being more interesting, because it contains two excitation terms while the TE wave has only one.

Let the incident plane wave be a known function of frequency $\phi(\omega)$:

$$E^i(\omega) = E_o \phi(\omega) \quad . \tag{3-18}$$

From (2-6) the total normal electric and tangential magnetic field on the metal surface are

$$E_y^{tot} = 2E_o \sin\theta \ \phi(\omega) \quad , \tag{3-19}$$

$$H_x^{tot} = - \frac{2E_o}{\eta} \sin\alpha \ \phi(\omega) \quad . \tag{3-20}$$

From (C-18) and (C-19), the transmission line sources ΔI and ΔV are

$$\Delta I = - \frac{1}{\sqrt{Z_o}} p_{ya} e_{yTEM}(x_o,0) \quad , \tag{3-21}$$

$$\Delta V = - \sqrt{Z_o} \ m_{xa} h_{xTEM}(x_o,0) \quad . \tag{3-22}$$

Dipole moments for circular aperture are given by (D-28) and (D-29). Since the coordinate system in Appendix D is different from the one which is used in Fig. 2-1, we have to exchange coordinates z and y as follows:

$$m_{xa} = j\frac{4}{3}\omega\mu \ a^3 \ H_x^{tot} \quad , \tag{3-23}$$

$$p_{ya} = j\frac{2}{3}\omega\varepsilon a^3 \ E_y^{tot} \quad . \tag{3-24}$$

The TEM-wave modal fields at the center of the aperture, in the absence of the aperture, are obtained from (B-12) and (B-13) as follows:

$$e_{yTEM}(x_o,0) = -\frac{\eta h}{\pi\sqrt{Z_o}(x_o^2 + h^2)} \quad , \tag{3-25}$$

$$h_{xTEM}(x_o,0) = \frac{h}{\pi\sqrt{Z_o}(x_o^2 + h^2)} \quad . \tag{3-26}$$

When substituted in (3-15), the above relations give the following values of P and M:

$$\left.\begin{matrix} P \\ M \end{matrix}\right\} = j\phi(\omega)\ (\sin\theta \pm 2\sin\alpha)\ \frac{4E_o hka^3}{3\sqrt{Z_o}\pi(x_o^2 + h^2)} \tag{3-27}$$

where the upper sign is for P and the lower sign is for M.

The voltages V_3 and V_4 are now obtained from (3-16) and (3-17) as follows

$$V_3(\omega) = \frac{2ha^2}{3\pi(x_o^2 + h^2)}\ E_o\phi(\omega)\ \phi_3(\omega) \quad , \tag{3-28}$$

$$V_4(\omega) = \frac{2ha^2}{3\pi(x_o^2 + h^2)}\ E_o\phi(\omega)\ \phi_4(\omega) \quad . \tag{3-29}$$

The frequency dependence is incorporated into the two functions denoted $\phi_3(\omega)$ and $\phi_4(\omega)$:

$$\phi_3(\omega) = jka(1+\rho_4)\ \frac{(\sin\phi + 2\sin\alpha)\ \rho_4 e^{-jk\ell}4 + (\sin\theta - 2\sin\alpha)e^{-jk\ell}4}{e^{jk\ell}tot - \rho_3\rho_4 e^{-jk\ell}tot} \quad , \tag{3-30}$$

$$\phi_4(\omega) = jka(1+\rho_4)\ \frac{(\sin\theta - 2\sin\alpha)\ \rho_3 e^{-jk\ell}3 + (\sin\theta + 2\sin\alpha)e^{jk\ell}3}{e^{jk\ell}tot - \rho_3\rho_4\ e^{-jk\ell}tot} \quad . \tag{3-31}$$

As the propagation constant is also a function of ω

$$k = \omega \sqrt{\mu\varepsilon} \quad , \qquad (3\text{-}32)$$

the above expressions may be used to compute the magnitude and phase of voltages V_3 and V_4 as functions of frequency. A following example has been selected:

aperture radius	$a = 10$ mm
distance from aperture to transm. line	$x_o = 20$ mm
transm. line radius	$r = 1$ mm
transm. line height	$d = 10$ mm
line length in (+z) direction	$\ell_4 = 2.1$ m
line length in (-z) direction	$\ell_3 = 3.0$ m
plane-wave angle of incidence	$\theta = 45^o$
azimuth angle for plane of incidence	$\alpha = 30^o$
load resistance at (+z) port	$R_4 = 10$ kΩ
load resistance at (-z) port	$R_3 = 10$ Ω

Assuming that the plane-wave spectrum is independent of frequency ($\phi(\omega)$=const), the relative voltage at the port 4, expressed in decibels, is shown in Fig. 3-2 as function of frequency. As seen from (3-31), at very low frequencies $k\ell_3 \ll 1$ and $k\ell_4 \ll 1$, so that $\phi_4(\omega)$ is proportional to ω. This situation prevails in Fig. 3-2 up to about 50 Mrad/s. At higher frequencies, the transmission line will have resonances determined by lengths ℓ_3 and ℓ_4 and by load values ρ_3 and ρ_4. As the characteristic impedance of the transmission line in the example chosen is Z_o=179Ω, port 3 is almost short-circuited by the resistance R_3=10Ω while port 4 is almost open-circuited. The first resonance occurs therefore at $k\ell_{tot}=\pi/2$ or

$$f_{res,1} = \frac{c}{4\ell_{tot}} = 14.9 \text{ MHz} = 92.4 \text{ Mrad/s} \quad ,$$

as can be seen in Fig, 3.2. Higher resonances occurring at

$$f_{res,n} = (2n+1) \cdot f_{res,1}$$

can be also seen in the same figure.

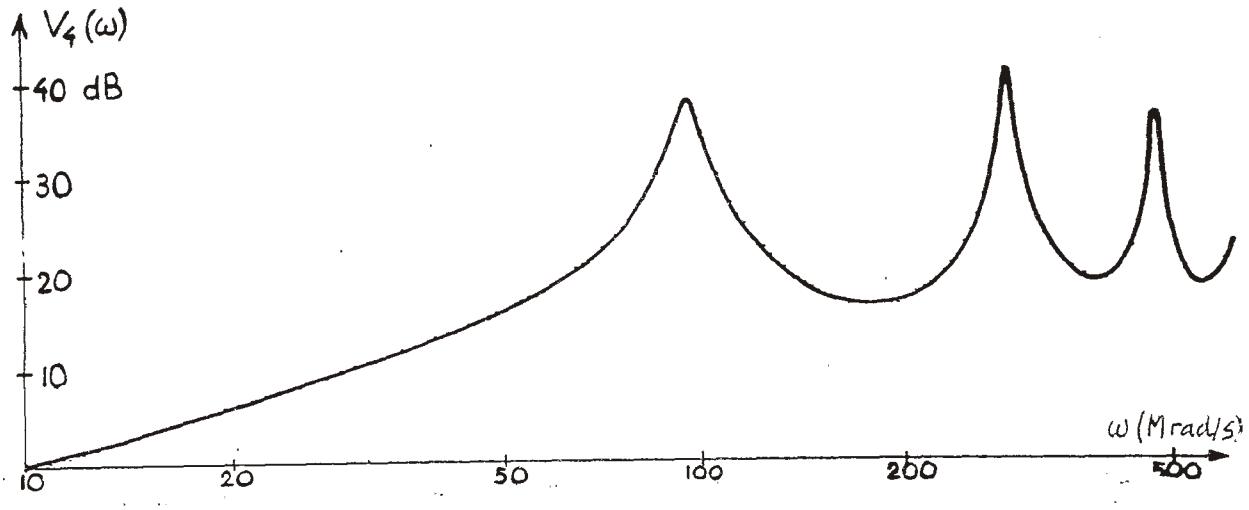

Fig. 3-2. Frequency response.

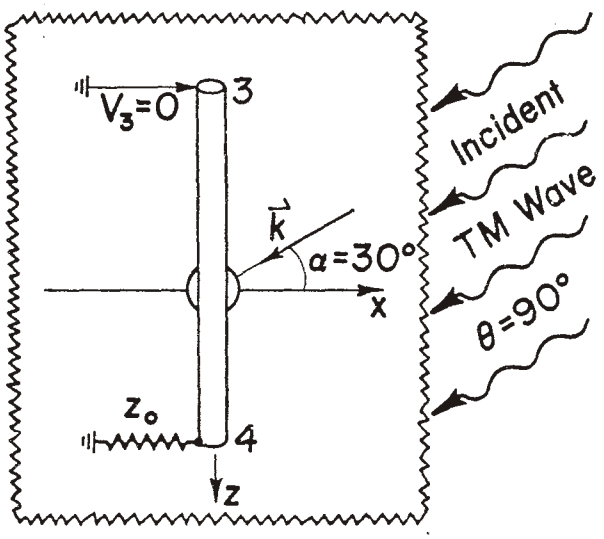

Fig. 3-3. Directional property of the aperture coupling: Voltage at port 3 is zero when azimuth is 30°.

An interesting directional property may be observed for the TM plane wave incident parallel with the ground plane. If the Port 4 is terminated in Z_o then one can see from (3-30) that $\phi_3=0$ when $\sin\theta=2\sin\alpha$ or, for $\theta=90^o$, when $\alpha=30^o$. As shown in Fig. 3-3, the voltage at port 3 will be zero, when the incident TM wave is coming under an angle $\alpha=30^o$, parallel with the ground plane. This property could be used to build a low-profile direction finder. However, a practical application of this effect is limited to strong incident waves only, because of the considerable signal loss at the passage through a small aperture.

In the example from p. 18 the lateral displacement of the hole x_o is larger than the wire height d. Therefore the assumption (D-9) is violated, and the neglection of the quadrupole term may cause an error in the obtained results. Fortunately, this error could have an influence only on the amplitudes of line voltages, whereas the frequency response and the time response are not affected by it.

When the hole is placed symmetrically beneath the wire as in Fig. 3-3 the assumption (D-9) is fulfilled and the neglection of the term $\partial H_{bx}/\partial x$ is well justified.

SECTION IV

Response in the Time Domain

The circuit model of the transmission line excitation through a small aperture is once again shown in Fig, 4-1. The sources ΔV and ΔI have been evaluated previously as functions of frequency. In this section, they will be expressed as functions of time. From (C-18) and (C-19)

$$\Delta I(t) = - \frac{1}{\sqrt{Z_o}} p_{ya} e_{yTEM}(x_o,0) \qquad (4\text{-}1)$$

$$\Delta V(t) = - \sqrt{Z_o}\, m_{xa} h_{xTEM}(x_o,0) \qquad (4\text{-}2)$$

Let a TM incident plane wave below the ground plane be a prescribed function of time

$$E_i(t) = A_o F(t) \quad . \qquad (4\text{-}3)$$

The corresponding total normal electric and tangential magnetic fields are obtained from (2-6):

$$E_y^{tot}(t) = 2A_o \sin\theta\ F(t) \quad , \qquad (4\text{-}4)$$

$$H_x^{tot}(t) = - \frac{2A_o}{\eta} \sin\alpha\ F(t) \quad . \qquad (4\text{-}5)$$

For a small circular aperture the magnetic and electric dipole moments in the frequency domain are given by (3-23) and (3-24). To obtain the time domain presentation, replace factor $j\omega$ by the time derivative d/dt:

$$m_{xa}(t) = \frac{4}{3} \mu a^3 \frac{dH_x^{tot}}{dt} \quad , \qquad (4\text{-}6)$$

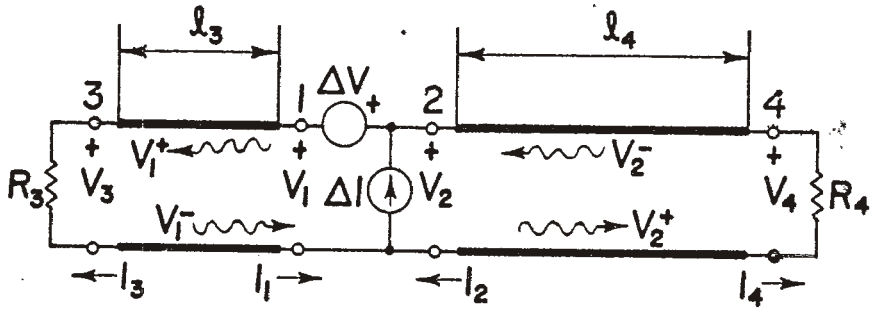

Fig. 4-1. Equivalent circuit for the transmission line.

$$p_{ya}(t) = \frac{2}{3}\,\varepsilon a^3\,\frac{dE_y^{tot}}{dt} \quad . \qquad (4\text{-}7)$$

Modal fields e_{yTEM} and h_{xTEM} do not depend on frequency or on time, as seen from (3-25) and (3-26). The sources ΔI and ΔV are therefore given by the following functions of time:

$$\Delta I(t) = \frac{\sin\theta}{Z_o} \cdot \frac{4ha^3A_o}{3\pi c(x_o^2+h^2)}\,F'(t) \quad , \qquad (4\text{-}8)$$

$$\Delta V(t) = 2\sin\alpha\,\frac{4ha^3A_o}{3\pi c(x_o^2+h^2)}\,F'(t) \quad , \qquad (4\text{-}9)$$

where $F'(t)$ stands for $dF(t)/dt$, and c is the velocity of light.

When the voltages and currents at ports 1 and 2 are decomposed in their incident and outgoing parts, like in (3-3), the Kirchhoff laws give the following

$$Z_o\Delta I(t) = V_1^+(t) - V_1^-(t) + V_2^+(t) - V_2^-(t) \quad , \qquad (4\text{-}10)$$

$$\Delta V(t) = -V_1^+(t) - V_1^-(t) + V_2^+(t) + V_2^-(t) \quad . \qquad (4\text{-}11)$$

TEM wave on a transmission line exhibits no dispersion: the waveforms travel along the line without deformation. E.g. the wave $V_2^+(t)$ travels toward the right-hand side of the line ℓ_4, and a portion of it is reflected back due to reflection coefficient ρ_4. When the reflected wave comes back to port 2, it is called $V_2^-(t)$:

$$V_2^-(t) = \rho_4 V_2^+(t-2\tau_4) \quad . \qquad (4\text{-}12)$$

Similarly, the reflected wave on the left-hand portion of the transmission line is

$$V_1^-(t) = \rho_3 V_1^+(t-2\tau_3) \quad . \qquad (4\text{-}13)$$

The time-shifts τ_3 and τ_4 are

$$\tau_3 = \frac{\ell_3}{c} \quad ; \quad \tau_4 = \frac{\ell_4}{c} \quad , \qquad (4\text{-}14)$$

as the TEM wave travels with the velocity of light c. Substitute (4-12) and (4-13) in (4-10) and (4-11) and obtain

$$V_1^+(t) = \tfrac{1}{2}[Z_o \Delta I(t) - \Delta V(t)] + \rho_4 V_2^+(t-2\tau_4) \quad , \qquad (4\text{-}15)$$

$$V_2^+(t) = \tfrac{1}{2}[Z_o \Delta I(t) + \Delta V(t)] + \rho_3 V_1^+(t-2\tau_3) \quad . \qquad (4\text{-}16)$$

The bracketed expressions in (4-15) and (4-16) are the sources which determine the shape and the magnitude of the transmission-line voltages. For shorter writing, denote these expressions by V_m and V_p as follows

$$V_m(t) = \frac{2ha^3 A_o}{3\pi c(x_o^2+h^2)} (\sin\theta - 2\sin\alpha)\, F'(t) \quad , \qquad (4\text{-}17)$$

$$V_p(t) = \frac{2ha^3 A_c}{3\pi c(x_o^2+h^2)} (\sin\theta + 2\sin\alpha)\, F'(t) \quad . \qquad (4\text{-}18)$$

By using this notation, the responses at ports 1 and 2 become

$$V_1^+(t) = V_m(t) + \rho_4 V_2^+(t-2\tau_4) \quad , \qquad (4\text{-}19)$$

$$V_2^+(t) = V_p(t) + \rho_3 V_1^+(t-2\tau_3) \quad . \qquad (4\text{-}20)$$

As seen from the above, the voltage responses on the transmission line are given by the time derivatives $F'(t)$ of the incident plane-wave time function $F(t)$, plus the terms originating from the reflections at the opposite sides of the transmission line.

One has obtained a pair of recurrence equations for computation of the time histories of $V_1^+(t)$ and $V_2^+(t)$. Assume that the incident

plane wave is a pulse starting at t=0. For $0 < t < 2\tau_4$, the voltage wave $V_1^+(t)$ in (4-19) is given only by $V_m(t)$, because the wave reflected from the port 4 has not yet arrived back to the point Z=0. The obtained expression for $V_1^+(t)$ should be shifted in time for $2\tau_3$, and added in (4-20), after a multiplication with ρ_3, etc.

The total time history of the back-and-forth reflections on the transmission line may be put in a graphical time table shown in Fig. 4-2. The example shown has the same dimensions as in Section 3, so that the time lag necessary for the wave emanating from the center to reach the port 4 is 7ns. The wavefront which started from the center toward the left and then comes back after a reflection at port 3, is shifted for 27ns, etc. The voltage observed at port 4 shows the arrival of these shifted pulses in a manner depicted in Fig. 4-3. Assuming that the line is lossless, the only loss of energy occurs when the wave is reflected from the resistive terminations at ports 3 and 4. If these terminations become lossless (like open-circuit or short circuit), the pulses bounce back and forth on the transmission line forever. On the other hand, when the ports 3 and 4 are terminated in matched loads, the pulses arrive at each end only once, and are totally dissipated there without any further reflection.

The following doubly-exponential function was selected as a typical incident waveform

$$F(t) = e^{-\alpha t} - e^{-\beta t} \qquad (4\text{-}21)$$

For the same example as in Section 3, the incident-wave parameters have been selected as follows:

incident wave magnitude	$A_o = 100\text{kV/m}$
short exponential	$\beta = 10^8 s^{-1}$
long exponential	$\alpha = 3 \cdot 10^6 s^{-1}$

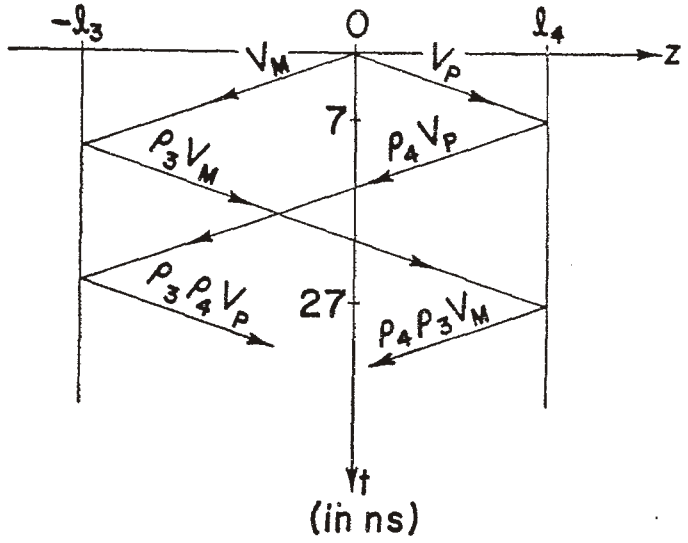

Fig. 4-2. Time table of wave reflections on the transmission line.

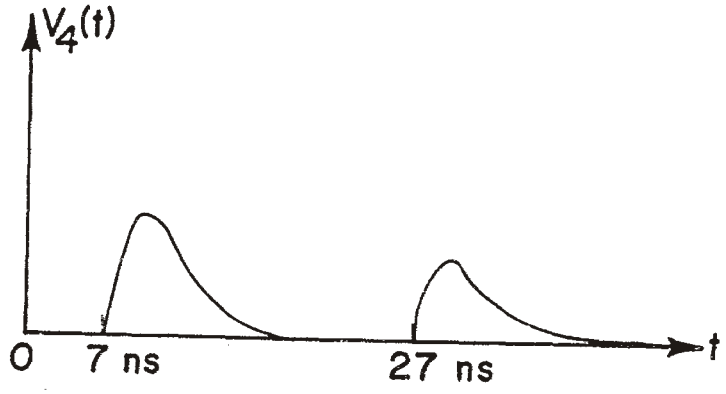

Fig. 4-3. General waveform at port 4.

The shape of the incident wave is shown in Fig. 4-4. Note the fast rise and the slow decay of this wave form. Also note that the value of F(t) is zero for negative times, which makes the derivative F'(t) discontinuous at t=0.

For the example selected in Section 3, the voltage at the port 4 is shown by a solid line in Fig. 4-5. This waveform is obtained from (4-19) and (4-20), while the time table from Fig. 4-2 was used for keeping track of the first nine arrivals at the port 4. It is important to note that the voltage appears in the form of a series of sharp spikes, which are gradually being attenuated due to lossy terminations at ports 3 and 4. The reason for the abrupt changes in $V_4(t)$ is the fact that the incident waveform F(t) has discontinuous derivatives, as mentioned above. The highest peak of the voltage V_4 is less than 0.5V, while the incident waveform has a strength of 100kV/m. This shows that an aperture of the radius of 1 cm allows very little of the incident energy to penetrate the hole.

The waveform in Fig. 4-5 is obtained by computing discrete values of $V_4(t)$ in increments of 1 ns. Due to the straight-line interpolation between the computed points, the plotted results seem as if the rise time of each of the pulses had the value 1 ns. Actually, this apparent finite rise-time is the consequence of the discretization in the computer output, while the actual rise-times are infinitesimally short. The same 1 ns discretization is selected in all the remaining illustrations.

Fig. 4-6 shows $V_4(t)$ when the termination at port 3 is equal to the characteristic impedance, namely $R_3=Z_o=179.5934\Omega$. It can be seen that the multiple reflections are no more present, and that the voltage consists of one single spike, of the same peak value as in Fig. 4-5.

In Fig. 4-7, both sides of the line are terminated in a matched load, $R_3=R_4=Z_o$. The wave shape is the same as in Fig. 4-6, but the peak value is about half smaller, since the total voltage

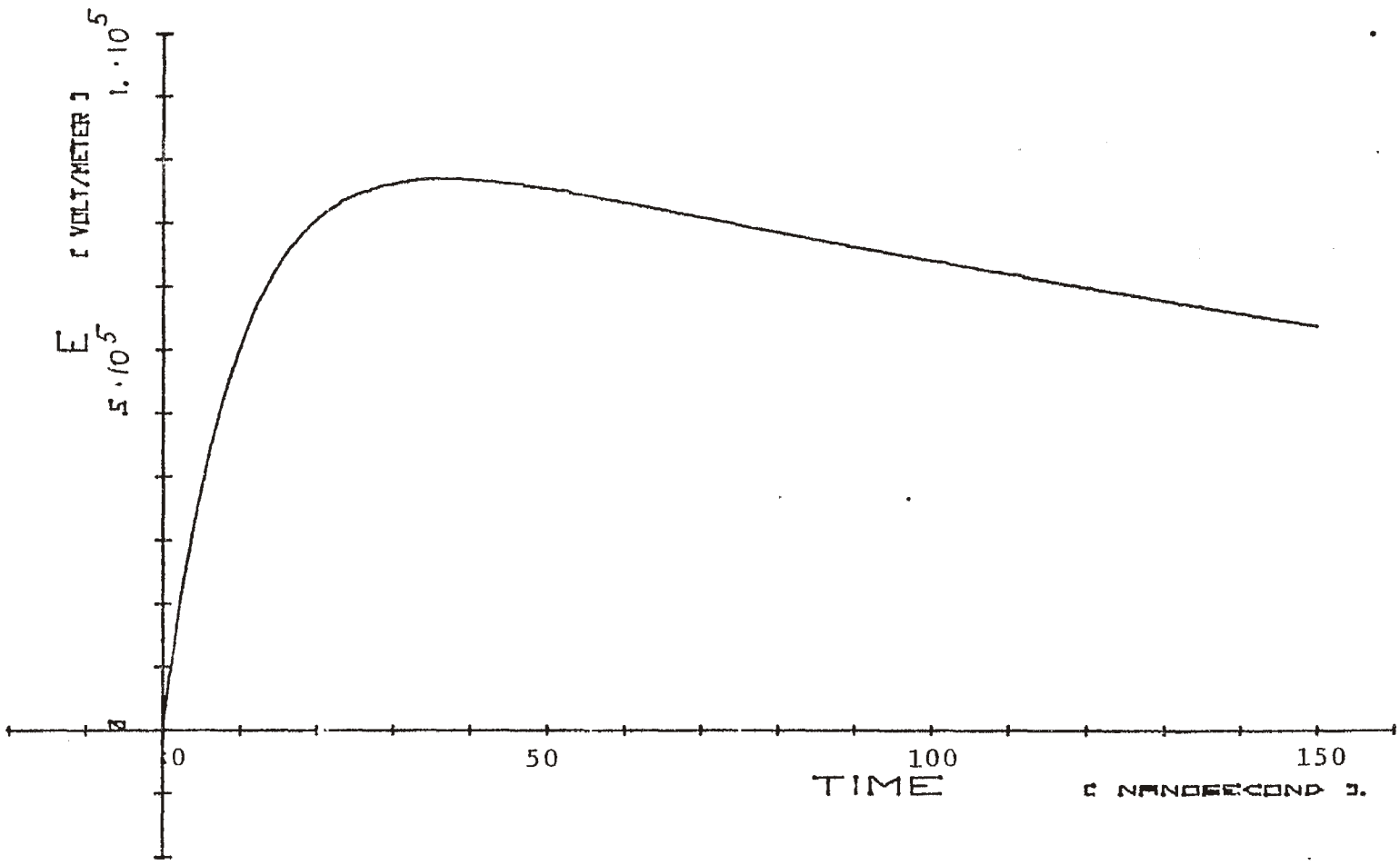

Fig. 4-4. Waveform of the incident wave.

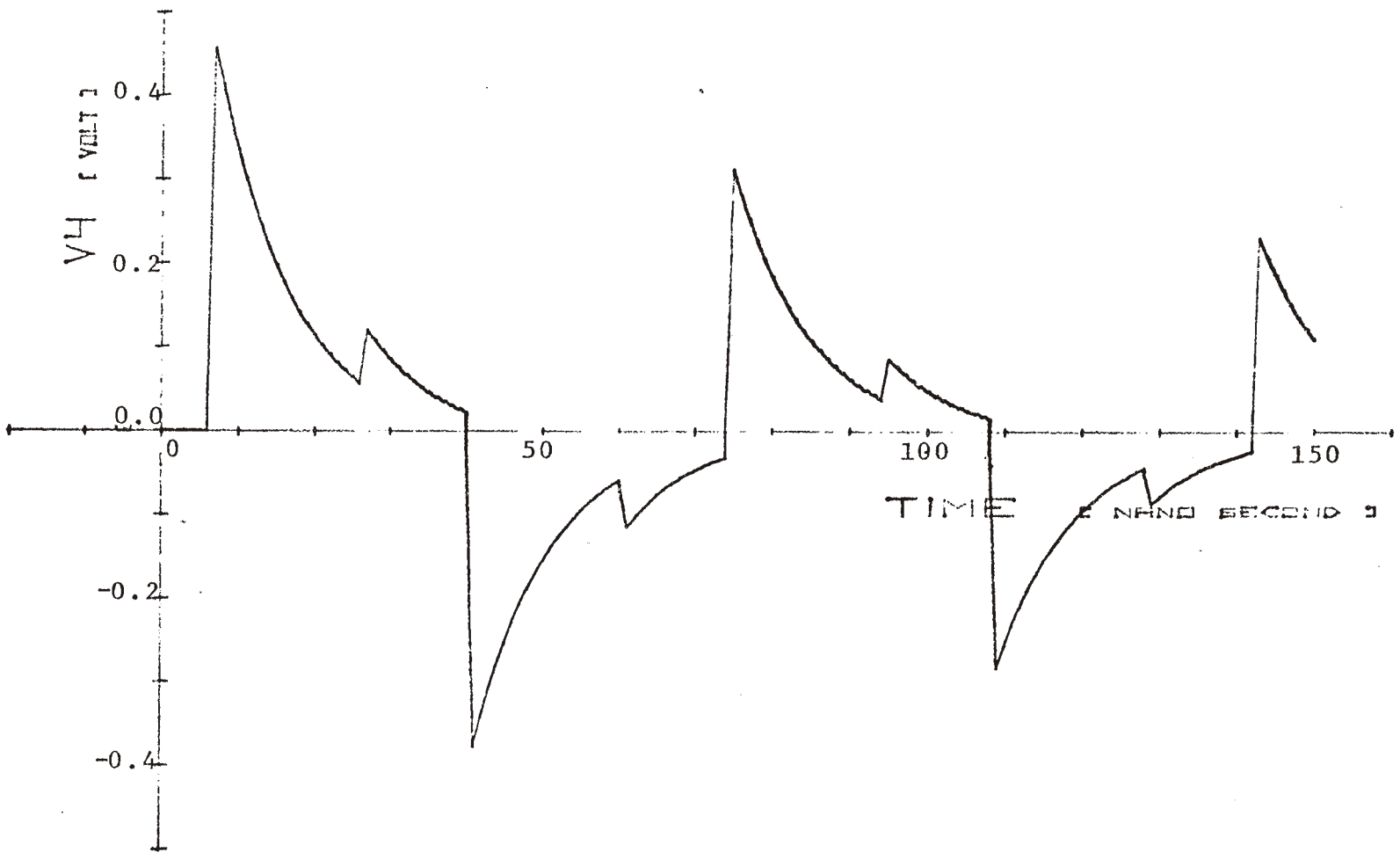

Fig. 4-5. Output voltage V_4 for R_3=10Ω, R_4=10kΩ, α=30°, θ=45°.

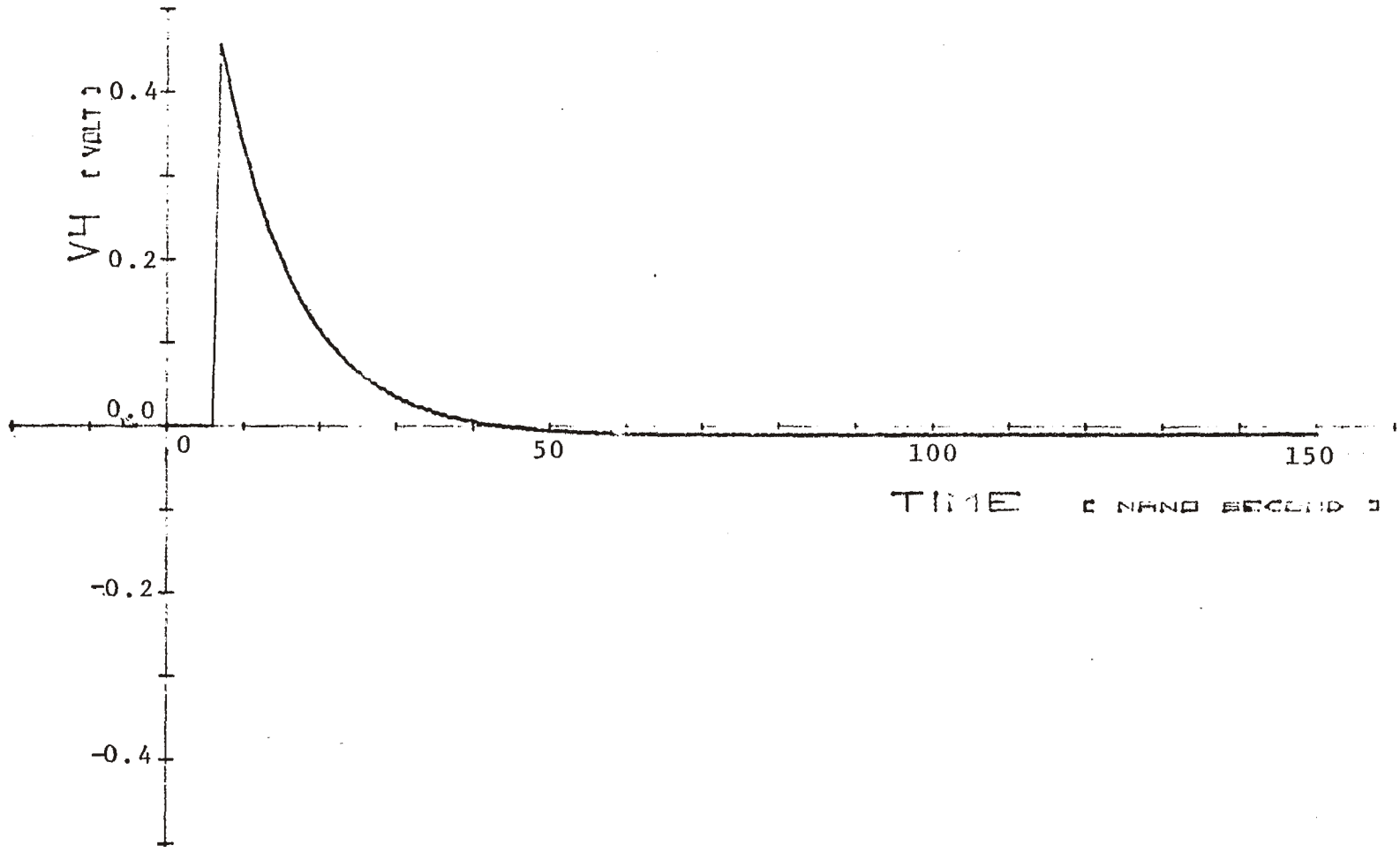

Fig. 4-6. Output voltage V_4 for R_3=179.59Ω, R_4=10kΩ, α=30°, θ=45°.

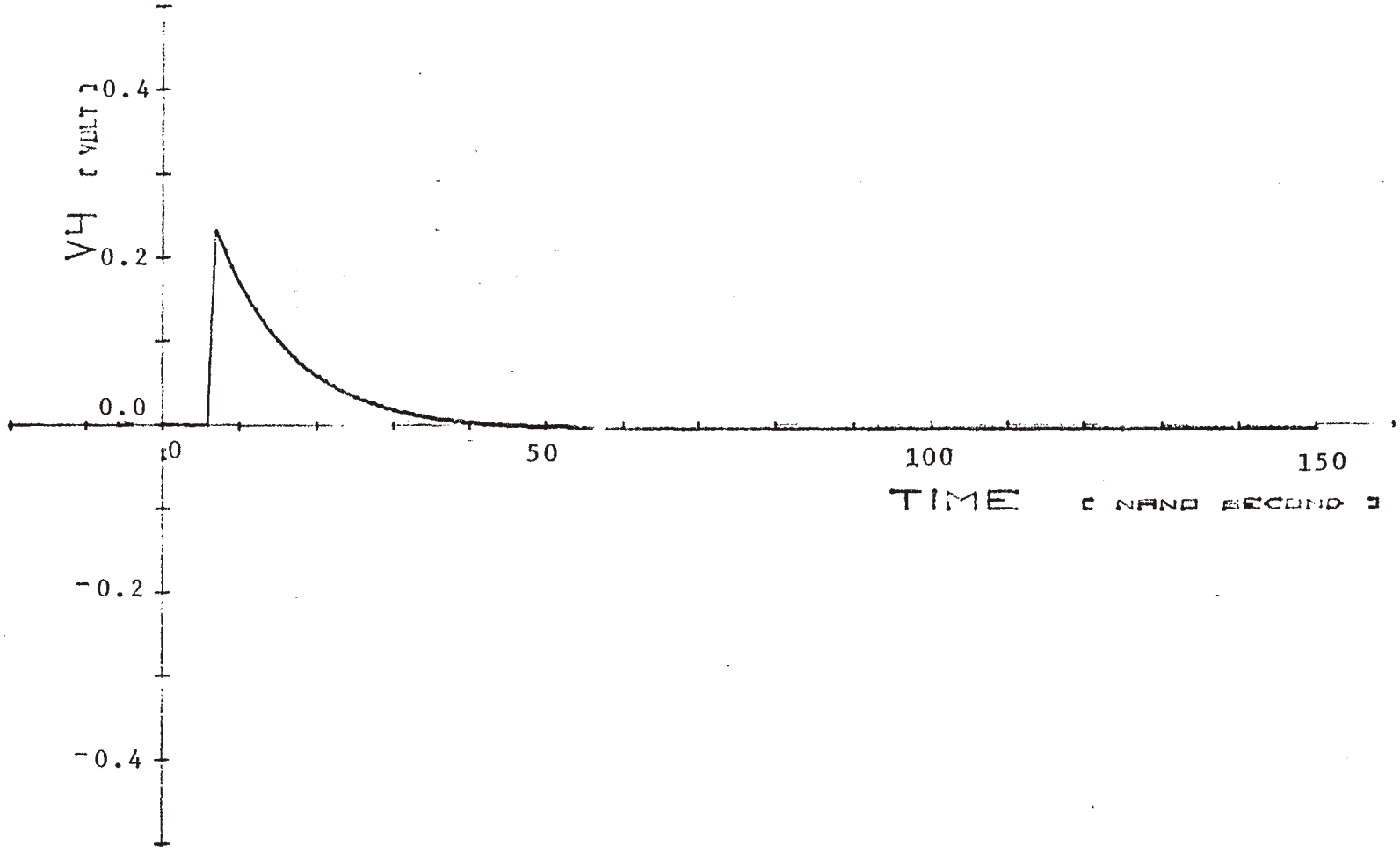

Fig. 4-7. Output voltage V_4 for $R_3=R_4=179.59\Omega$, $\alpha=30^{o}$, $\theta=45^{o}$.

at port 4 consists of the incident wave only, while in Fig. 4-6 both incident and reflected waves were present.

In Figs. 4-8 through 4-10 the terminations are again mismatched: $R_3=10\Omega$ and $R_4=10k\Omega$. This time the angle of incidence θ is varied. Note that in Fig. 4-5, $\theta=45^\circ$. This situation is to be compared with $\theta=0^\circ$ in Fig. 4-8, $\theta=60^\circ$ in Fig. 4-9 and $\theta=90^\circ$ in Fig. 4-10. Obviously, the two functions V_p and V_m from (4-17) and (4-18) depend on θ, so that the outgoing waves $V_1^{\mp}$ and V_2^{+} from (4-19) and (4-20) also depend on θ. As one can see, for $\theta=0^\circ$ the two waves V_1^{+} and V_2^{+} have about the same amplitude. At $\theta=60^\circ$ V_2^{+} is much greater than V_1^{+}, while at $\theta=90^\circ$ V_1^{+} is equal to zero, and only V_2^{+} exists. This demonstrates the directional behavior of the hole coupling, which was mentioned at the end of Section 3. Only the wave V_2^{+} exists, which travels toward the port 4, it is then reflected back because $R_4>>Z_o$, travels back toward port 3, it is reflected with the opposite sign since $R_3<<Z_o$, etc.

Figures 4-11 through 4-13 give an illustration of how sensitive is the directional property to slight variations of different parameters. In all these three figures $\theta=90^\circ$ and α is close to -30°, so that the directional property is demonstrated. For the purposes of direct comparison, the voltage scale is the same as in previous figures. In Fig. 4-11 the termination at port 3 is close to matched value, $R_3=200\Omega$, the termination at port 4 is almost open circuit, $R_4=10k\Omega$, and $\alpha=-30^\circ$. As seen in the figure, the first pulse arrives at t=27ns. This is a pulse reflected from the port 3 which is not exactly matched, and the peak value of the pulse is well below 0.1V. There is no direct arrival at t=7ns, because of the directive property of the hole. Also, second reflection is so small that it is not visible in the selected scale. In Figs. 4-12 and 4-13 the termination at the port 3 is exact, $R_3=179.5934\Omega$. When $\alpha=-30^\circ$, there is no output at port 4, as shown in Fig. 4-12. However, for slightly different orientation $\alpha=-25^\circ$, the small pulse appears at t-7ns, as shown in Fig. 4-13.

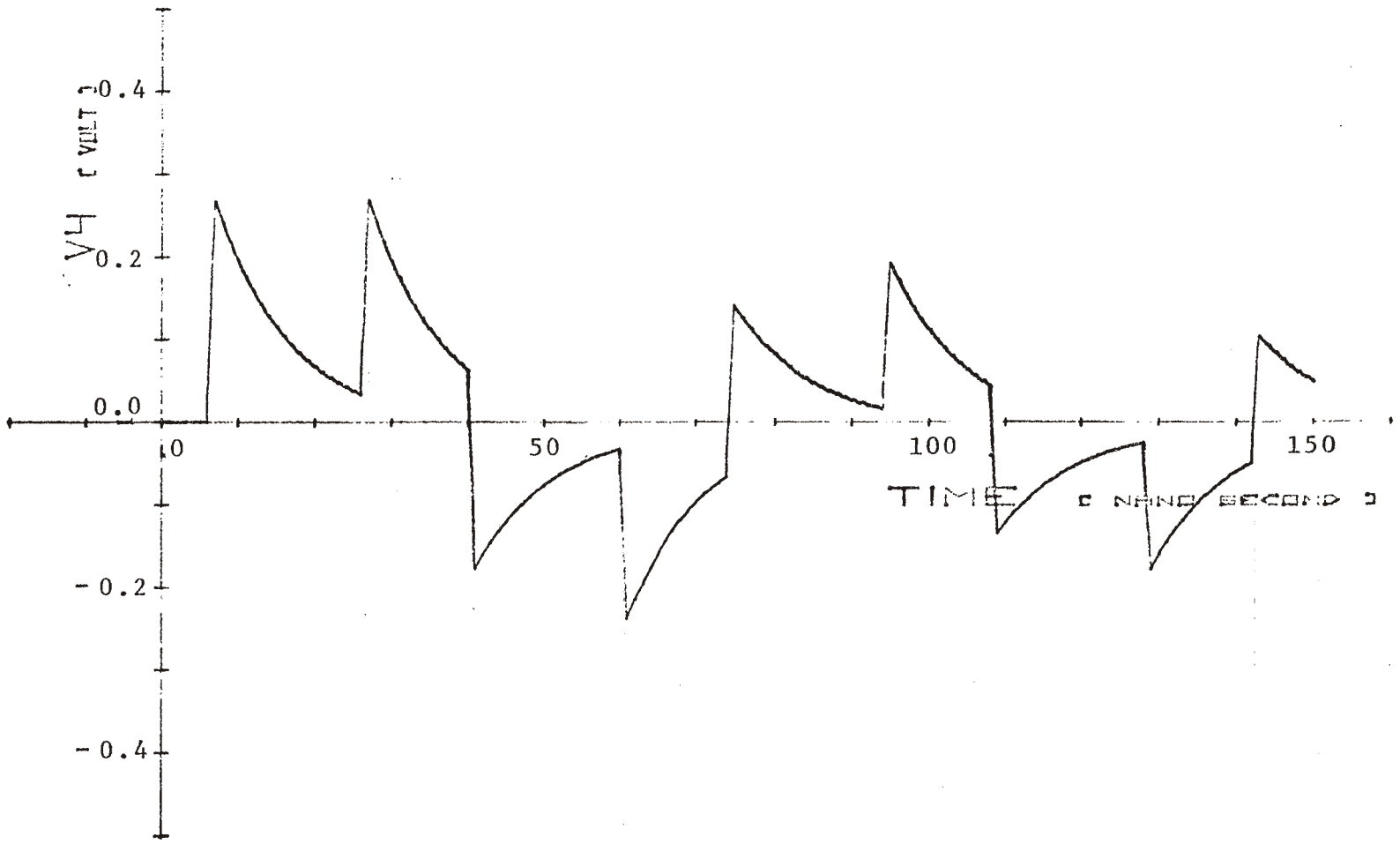

Fig. 4-8. Output voltage V_4 for R_3=10Ω, R_4=10kΩ, α=30°, θ=0°.

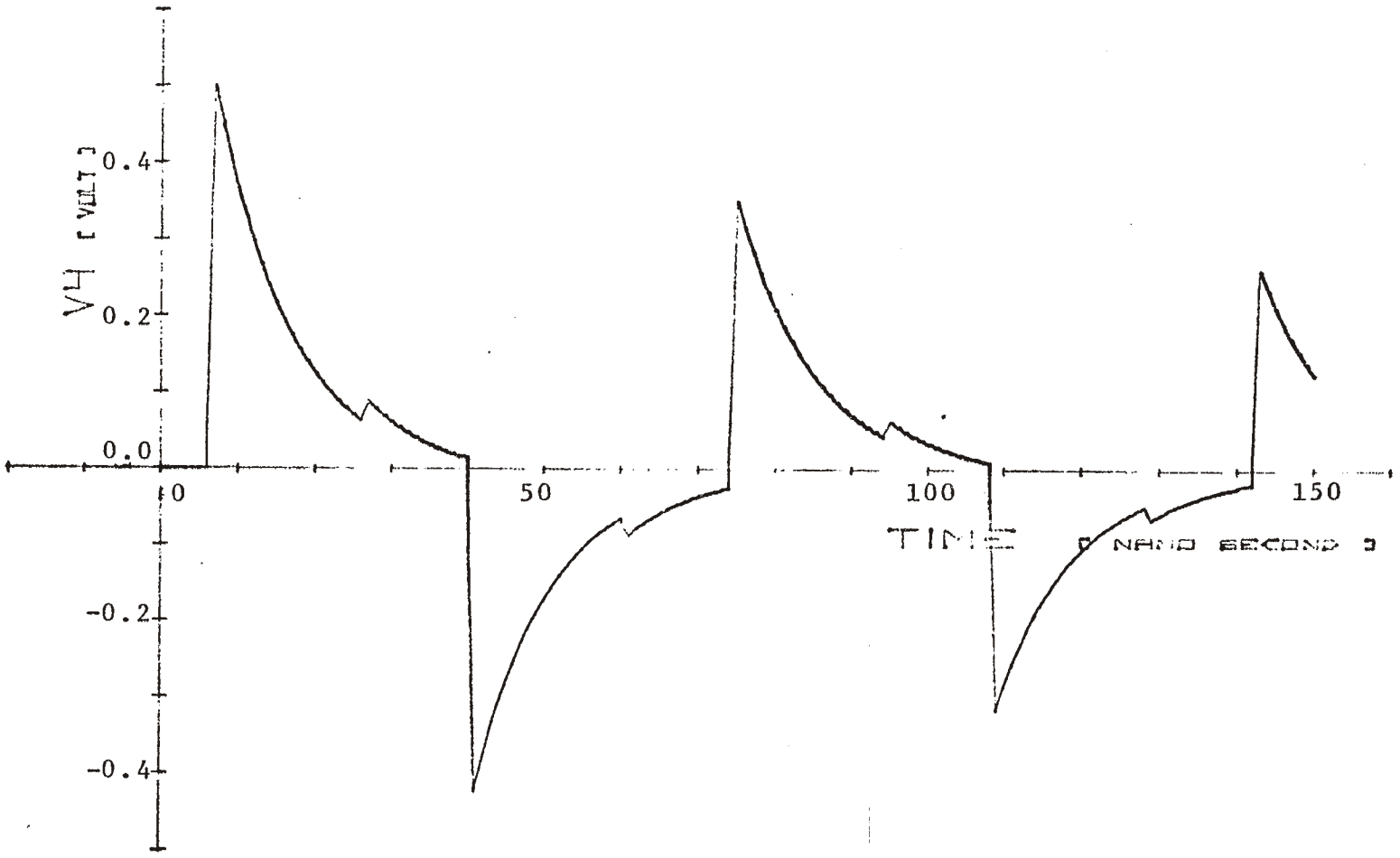

Fig. 4-9. Output voltage V_4 for R_3=10Ω, R_4=10kΩ, α=30°, θ=60°.

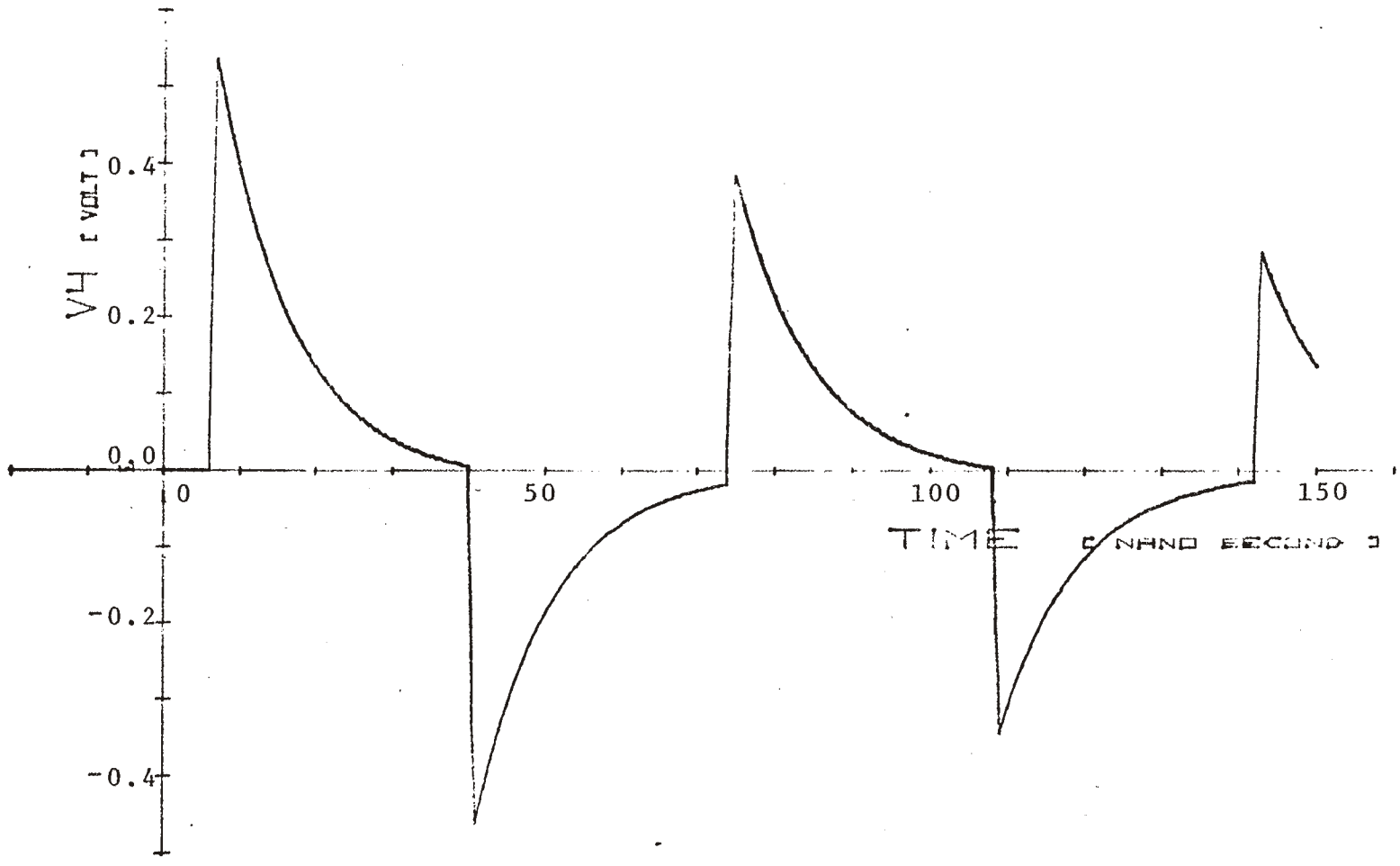

Fig. 4-10. Output voltage V_4 for R_3=10Ω, R_4=10kΩ, α=30°, θ=90°.

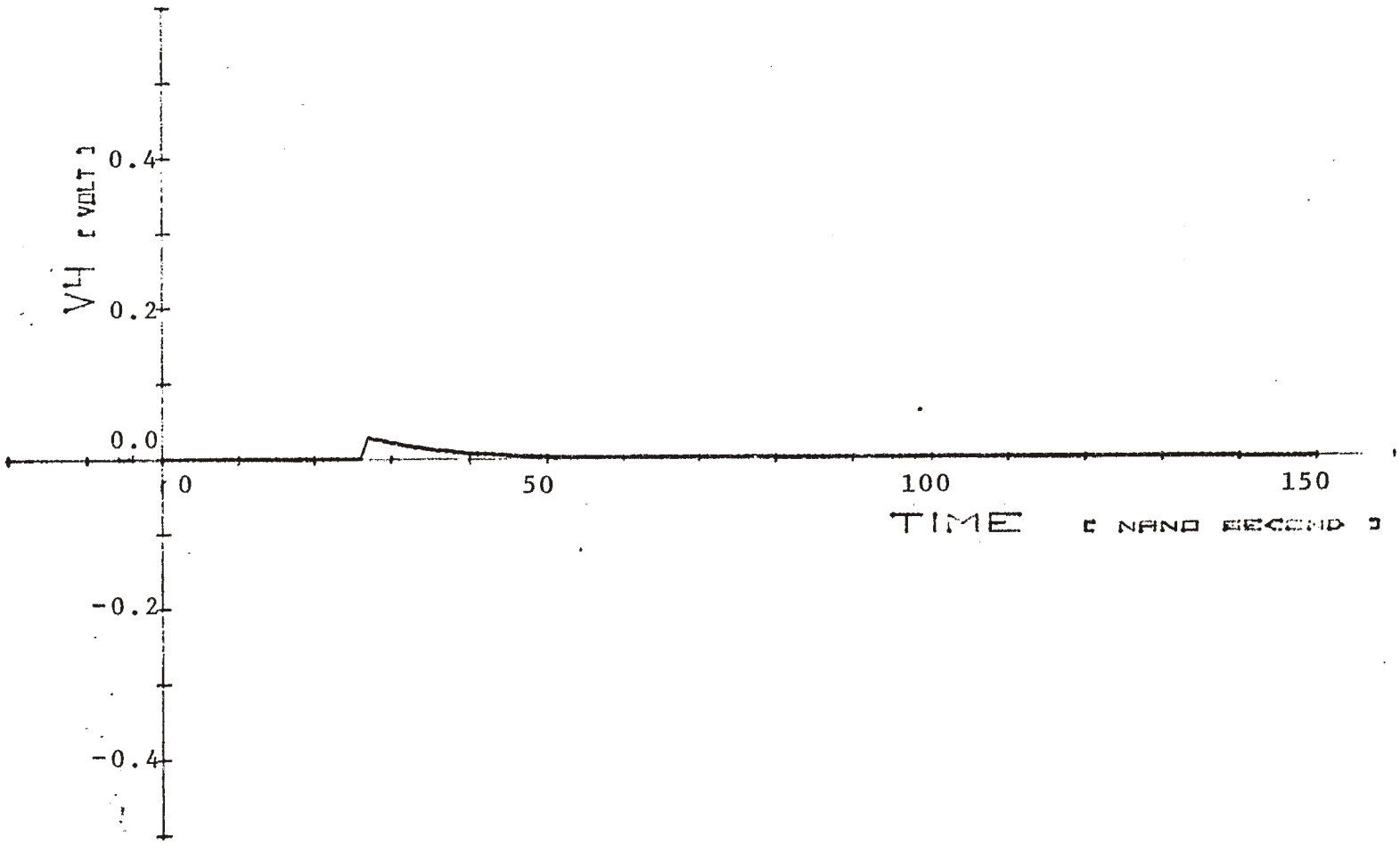

Fig. 4-11. Output voltage V_4 for R_3=200Ω, R_4=10kΩ, α=-30°, θ=90°.

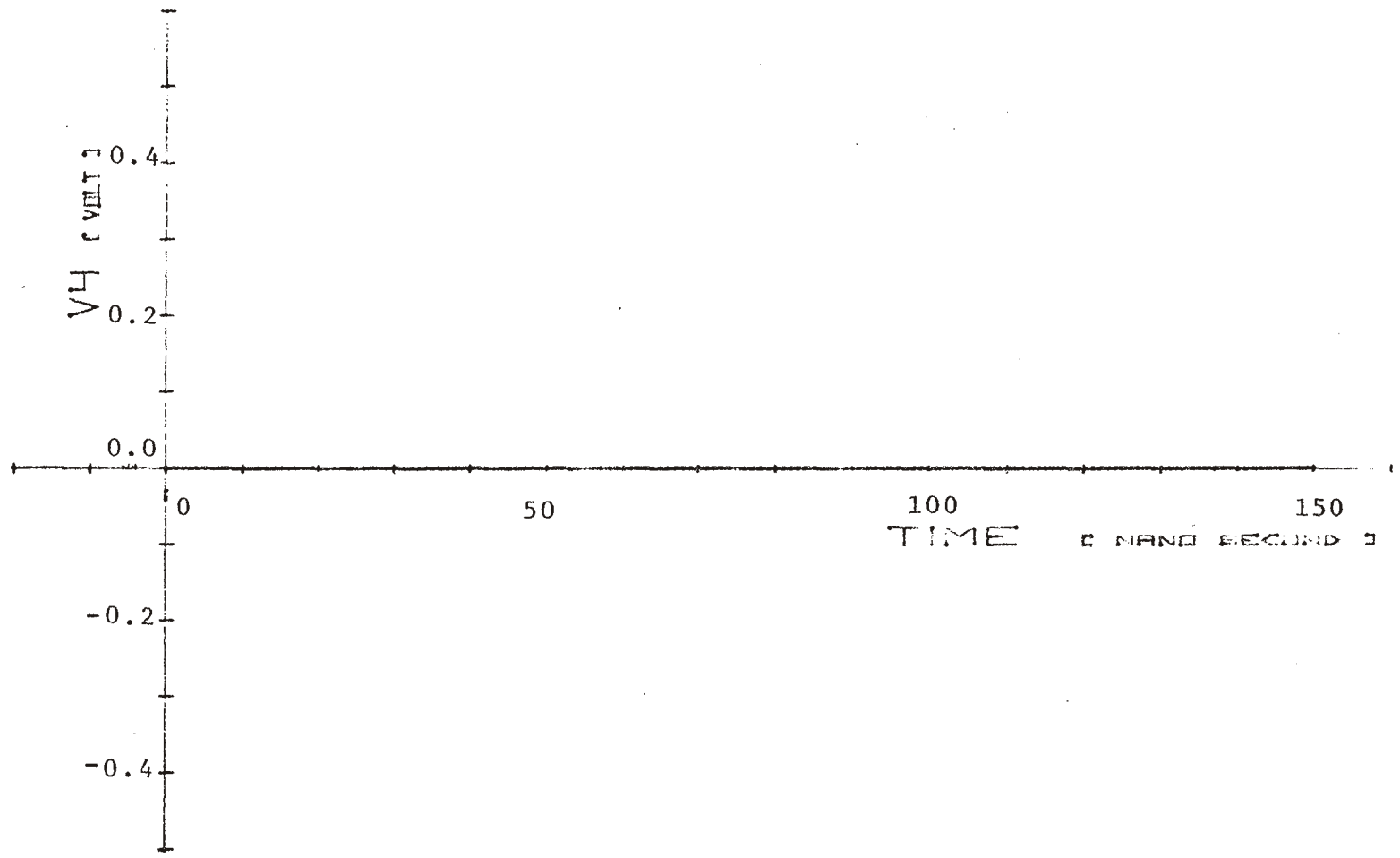

Fig. 4-12. Output voltage V_4 for R_3=179.59Ω, R_4=10kΩ, α=-30°, θ=90°.

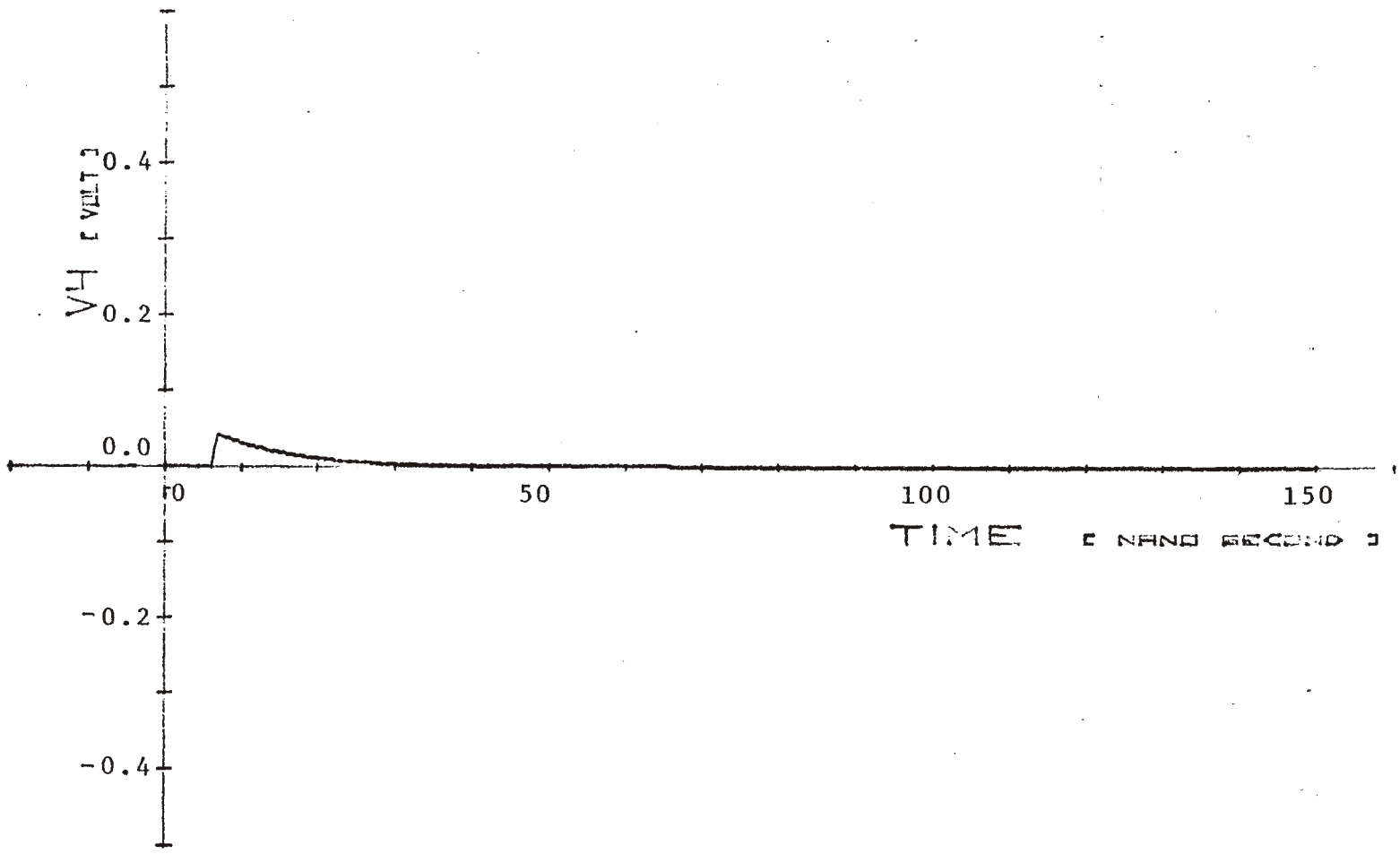

Fig. 4-13. Output voltage V_4 for R_3=179.59Ω, R_4=10kΩ, α=-25°, θ=90°.

In the examples presented above, the voltage at port 4 was about double of the incident-wave voltage, because port 4 was essentially open circuited. This voltage becomes much smaller if the port is essentially short-circuited. In Fig. 4-14 all the parameters are the same as in Fig. 4-5, except that R_4=10Ω, which is much smaller than Z_o. Obviously, the incident and the reflected voltage waves at port 4 are now of the opposite sign, so that the total voltage is small . Fig. 4-15 is obtained when the terminations on both sides of the transmission line are approximately open circuits: R_3=R_4=10kΩ. When this situation is compared with Fig. 4-5, it can be seen that the first arrival at t=7ns has the same polarity as before, while the second arrival at t=27ns has the reversed polarity. The resulting waveshape is thus strongly dependent on the value of the terminating resistances.

Instead of using the direct approach for computation of the time response as in this section, it is possible to obtain the time response by taking a Fourier transform of the frequency response obtained in Section 3. This has been done for the same example treated here, and the results are shown in Fig. 4-16. This waveform has been obtained by using a Fast Fourier Transform subroutine FOURI, with N=2048 points, spaced 1 ns apart. Only the first 180 points are shown in the illustration, the rest of them are needed only to provide enough time for the waveform to die out. As expected, the waveform reconstructed from the Fourier transform does not have as sharp edges as the original but otherwise, the similarity between Figures 4-5 and 4-16 is very good.

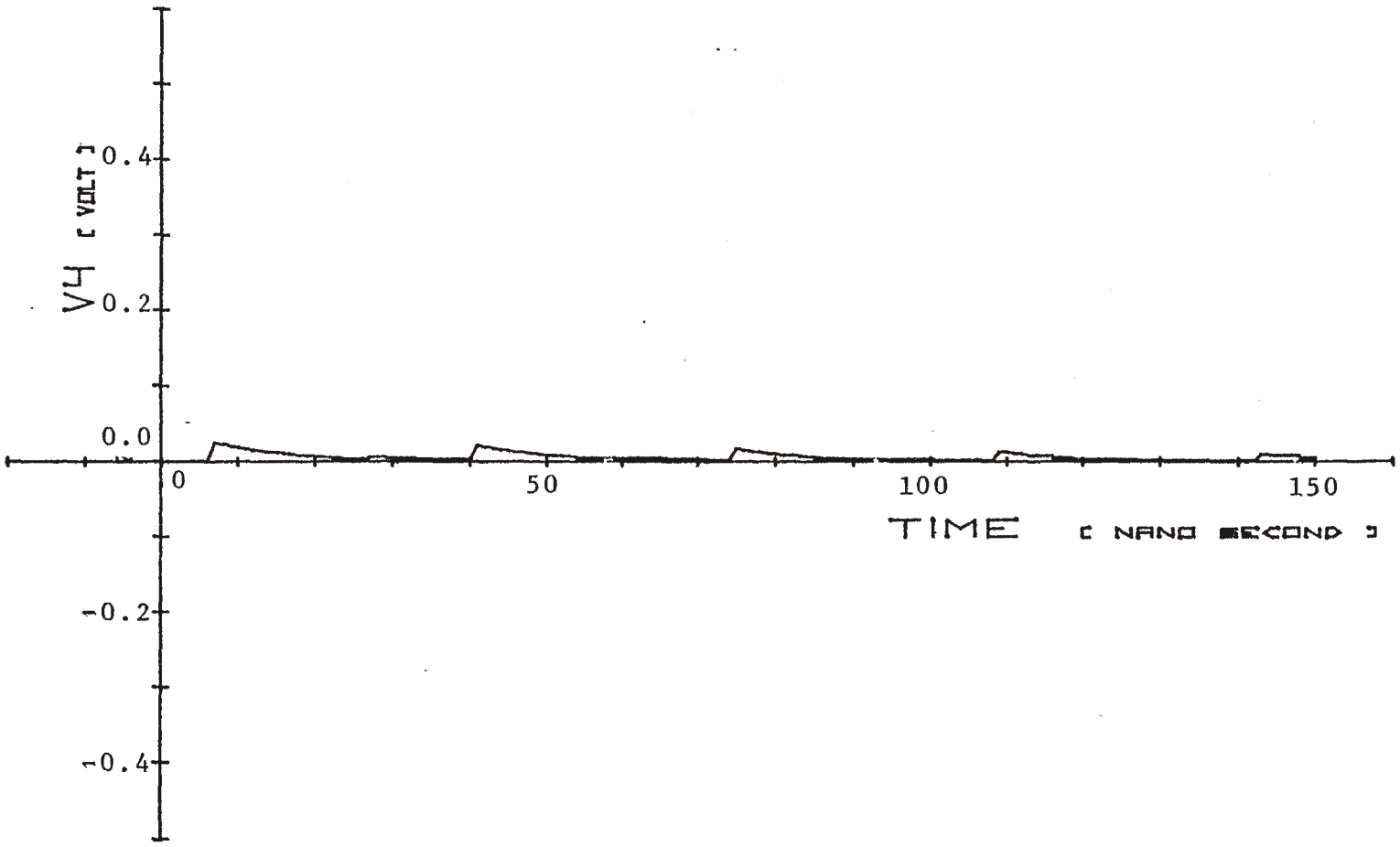

Fig. 4-14. Output voltage V_4 for $R_3=10\Omega$, $R_4=10\Omega$, $\alpha=30^{\circ}$, $\theta=45^{\circ}$.

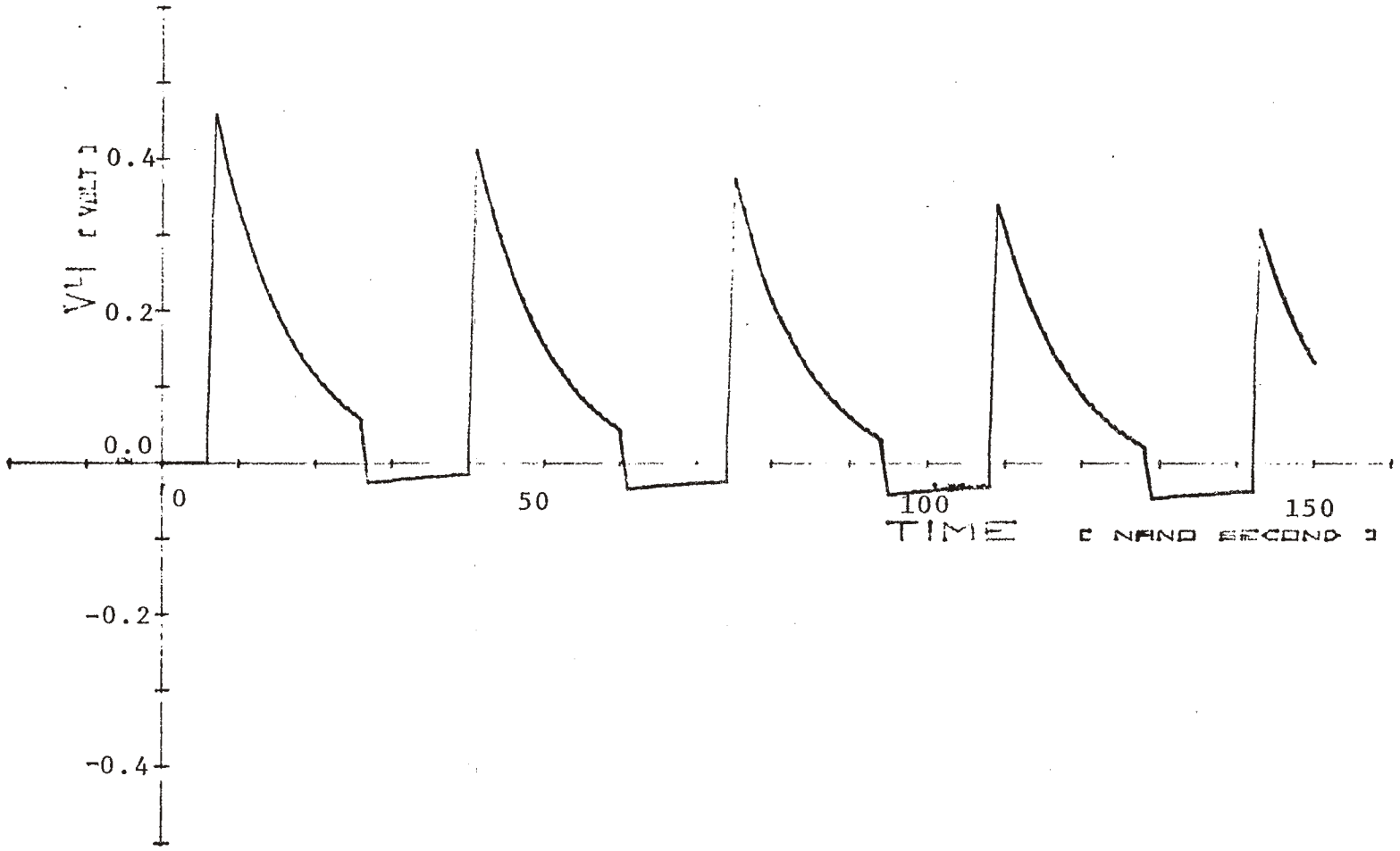

Fig. 4-15. Output voltage V_4 for R_3=10kΩ, R_4=10kΩ, α=30°, θ=45°.

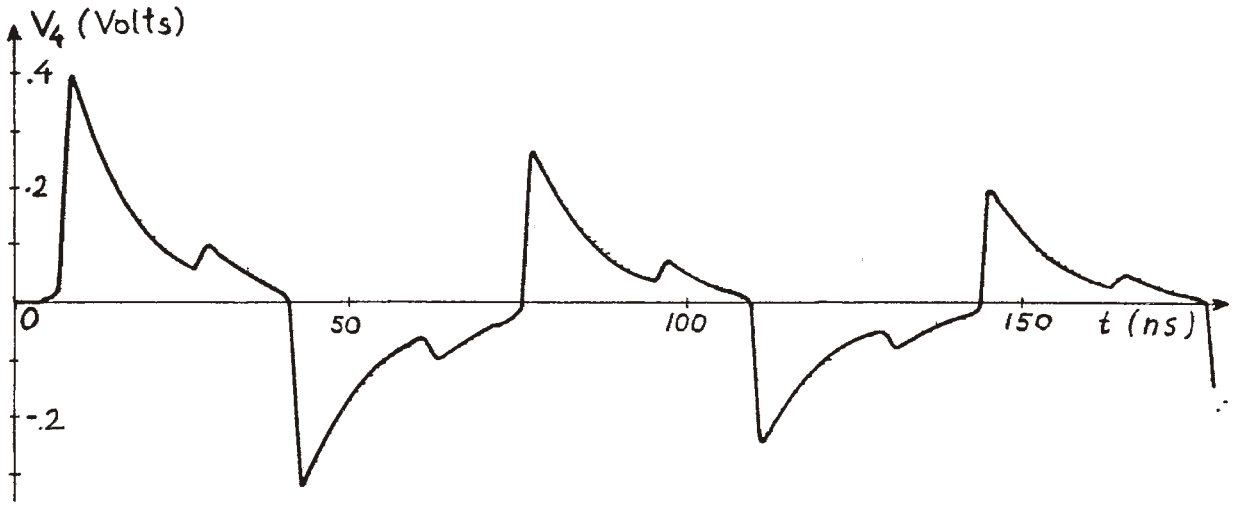

Fig. 4-16. Output voltage V_4 obtained by the FOURIER Transform.

APPENDIX A

TEM Field of a Circular Wire Above the Ground Plane

In Fig, A-1(a), a line charge of q Coulombs per meter is placed at height h above the infinite ground plane. At the observation point P, the electrostatic potential ϕ can be computed from (see [A.1])

$$\phi = \frac{q}{2\pi\epsilon} \ln \left(\frac{r_2}{r_1}\right) \tag{A-1}$$

where the potential of the ground plane was taken to be zero.

A dynamic electric field of a TEM wave may be obtained from the above potential ϕ by taking the transverse gradient operator ∇_t as follows (see [A.2])

$$\vec{E} = -\nabla_t \phi e^{-jkz} \quad . \tag{A-2}$$

For the geometry from Fig. A-1a, the above equation yields the following components of the electric field in rectangular coordinates:

$$E_x = \frac{qh}{\pi\epsilon} \cdot \frac{2xy}{[x^2+(y-h)^2][x^2+(y+h)^2]} e^{-jkz} \quad , \tag{A-3}$$

$$E_y = -\frac{qh}{\pi\epsilon} \cdot \frac{h^2+x^2-y^2}{[x^2+(y-h)^2][x^2+(y+h)^2]} e^{-jkz} \quad . \tag{A-4}$$

The equipotential lines of this field are eccentric circles [A.1]. Therefore, the same field is an exact representation for a metal circular cylinder of a finite radius r above the ground plane, as shown in Fig. A-1(b). Note that the center of this cylinder is not at the height h above the ground plane, but at a

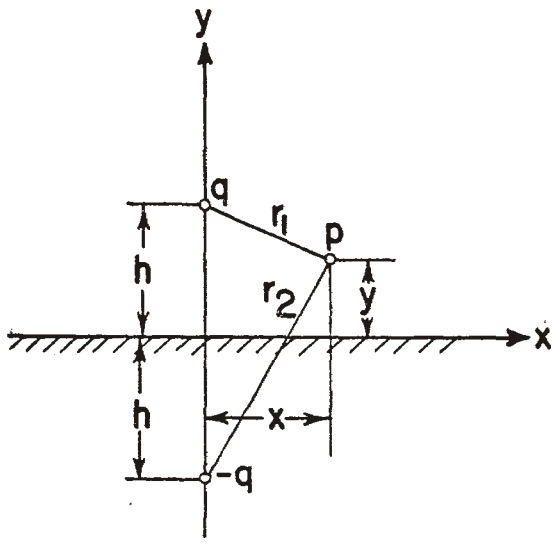

Fig. A-1a. Line source above the ground plane.

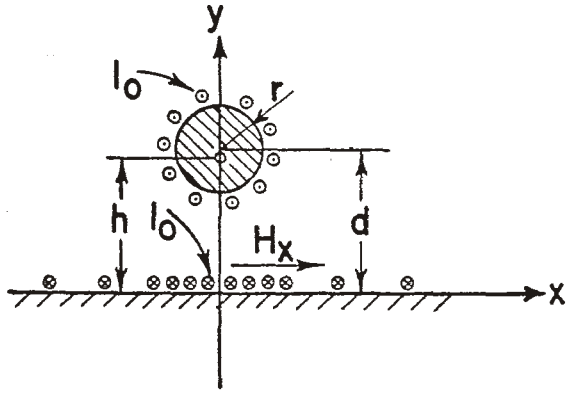

Fig. A-1b. Circular cylinder above the ground plane.

different height, denoted d [A.1]

$$d^2 = h^2 + r^2 \quad . \tag{A-5}$$

The potential difference between the ground plane and the surface of the cylinder is, due to conservative property of the TEM field,

$$V_o = -\int_{y=0}^{y=d-r} E_y(0,y)\,dy = \frac{q}{2\pi\epsilon} \ln \left(\frac{h+d-r}{h-d+r}\right) \quad . \tag{A-6}$$

After some manipulation (see e.g. [A-3] for details), (A-6) can be brought to the following form

$$V_o = \frac{q}{2\pi\epsilon} \cosh^{-1} \left(\frac{d}{r}\right) \quad . \tag{A-7}$$

When (A-7) is used to express q in terms of V_o, the expressions for the electric field components (A-3) and (A-4) become

$$E_x = \frac{4hV_o}{\cosh^{-1}\left(\frac{d}{r}\right)} \cdot \frac{xy}{[x^2+(y-h)^2][x^2+(y+h)^2]} e^{-jkz} \quad , \tag{A-8}$$

$$E_y = -\frac{4hV_o}{\cosh^{-1}\left(\frac{d}{r}\right)} \cdot \frac{h^2+x^2-y^2}{[x^2+(y-h)^2][x^2+(y+h)^2]} e^{-jkz} \quad . \tag{A-9}$$

In the above formulas, h is to be computed from physical dimensions d and r by using (A-5), and V_o is the voltage between the cylindrical conductor and the ground plane.

The corresponding magnetic field can be found from Maxwell's equation

$$-j\omega\mu \vec{H} = \bar{\nabla} \times \vec{E} \quad . \tag{A-10}$$

When the components of $\vec{H}$ are evaluated in rectangular coordinates, the result is

$$H_x = -\frac{E_y}{\eta} \quad , \quad H_y = \frac{E_x}{\eta} \quad , \qquad \text{(A-11)}$$

where $\eta = \sqrt{\mu/\epsilon} = 120\pi$ in air.

For a TEM wave traveling in +z direction, the voltage between the conductor and ground is V_o. The total current I_o on the conductor can be obtained from (see Fig. A-1b)

$$I_o = \int_{-\infty}^{\infty} H_x(x,0)dx = \frac{2\pi V_o}{\eta \cosh^{-1}(\frac{d}{r})} \quad . \qquad \text{(A-12)}$$

Therefore, the characteristic impedance of the air-filled transmission line from Fig. A-1b is

$$Z_o = \frac{V_o}{I_o} = 60 \cosh^{-1}(\frac{d}{r}) \quad . \qquad \text{(A-13)}$$

Note that all the above equations are exact, valid for any dimensions d and r, as long as the conductors may be assumed to have perfect conductivity.

APPENDIX B

Coupling Coefficients for TEM Mode Excited by Localized Current Sources. (Reciprocity Theorem Method)

Figure B-1 represents a general waveguide in which there is a localized current source $\vec{J}$. This source is capable of producing outgoing waves which carry away the energy across the distant "ports" located at z_1 and z_2. For the n-th outward propagating mode, the wave amplitudes and phases are denoted by C_n^- and C_n^+ according to Collin [B.1]. The total electric and magnetic field of the outgoing wave at the position z_2 will be a sum of all the propagating modes:

$$\vec{E}^+ = \sum_{n=1}^{\infty} C_n^+ (\vec{e}_n + \vec{e}_{zn})\, e^{-j\beta_n z_2} \quad , \qquad \text{(B-1)}$$

$$\vec{H}^+ = \sum_{n=1}^{\infty} C_n^+ (\vec{h}_n + \vec{h}_{zn})\, e^{-j\beta_n z_2} \quad . \qquad \text{(B-2)}$$

The above notation is taken from Collin. $\vec{e}_n$ and $\vec{h}_n$ are real functions, representing normalized transverse electric and magnetic fields of the n-th mode. The normalization is here taken to be such that

$$\int_{\text{cross section}} (\vec{e}_n \times \vec{h}_n) \cdot d\vec{S} = 1 \quad . \qquad \text{(B-3)}$$

Instead of unity, the above integral may be set equal to an arbitrary constant as in Collin, but the choice (B-3) seems to be more convenient here.

Under the assumption that the individual modes are mutually orthogonal, i.e.

$$\int_{\text{cross section}} (\vec{e}_m \times \vec{h}_n) \cdot d\vec{S} = 0 \text{ for } n \neq m \quad , \qquad \text{(B-4)}$$

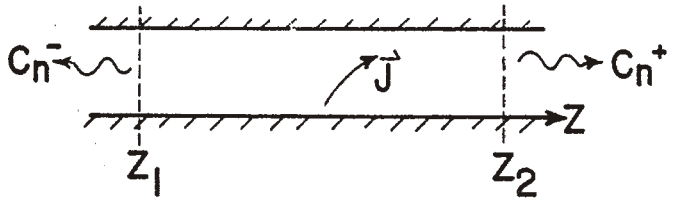

Fig. B-1. Waveguide excitation by a current source $\vec{J}$.

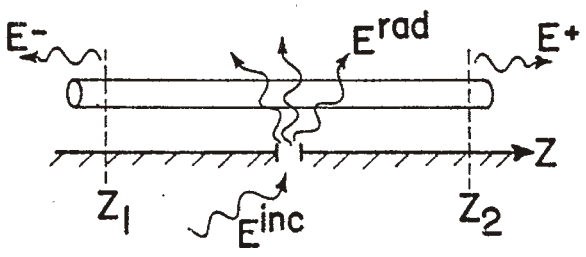

Fig. B-2. Incident and scattered waves for the open region.

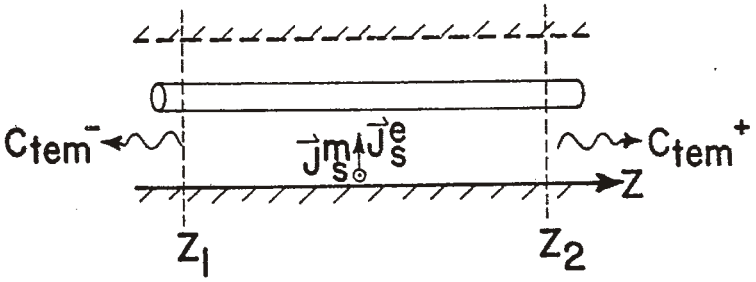

Fig. B-3. Fictitious upper ground plane closes the region.

Collin [B.1] applied the reciprocity theorem to the situation shown in Fig. B-1 in order to derive the simple rule for computation of the amplitude C_n^+ of the outgoing n-th modal wave:

$$-2C_n^+ = \int_V (\vec{e}_n - \vec{e}_{zn}) \cdot \vec{J} e^{j\beta_n z} dV \quad . \qquad \text{(B-5)}$$

Therefore, the rule is to take the electric field of the n-th modal wave traveling in negative z direction and form the scalar product of this field with the current source $\vec{J}$. The integration is to be performed over the volume V within which the current $\vec{J}$ exists. C_n^+ is a wave amplitude of the wave traveling in the positive z direction, as shown in Fig. B-1.

The above rule will be next applied to the particular problem of energy coupling from the small aperture to the single-wire transmission line, as shown in Fig. B-2. The incident wave coming from below the ground plane produces a given field configuration over the aperture. This field in turn causes the energy transfer into a region above the ground plane by two distinct mechanisms: a direct radiation into a free space above the ground plane (denoted by E^{rad} in Fig. B-2), and a guided TEM wave propagation along the wire (denoted by E^+ and E^- in the same figure).

In this study one is primarily interested in the guided energy propagating along the transmission line. In order to make this problem directly amenable to the application of the rule (B-5), one may imagine another ground plane somewhere above the wire, so that the energy can propagate away from the aperture only be means of guided waves, traveling in positive and negative z directions. This second ground plane is indicated by a dotted line in Fig. B-3. In actual practical situations, this additional ground plane is formed by the other side of an airplane wing, as indicated in Fig. B-4.

Appendix D describes the method of replacing the aperture in a ground plane with a lid in the ground plane over which there is situated a pair of electric and magnetic dipoles. The ground

plane is now completely closed as shown in Fig. B-3, and the current source consists of two dipoles $\vec{J}_s^m$ and $\vec{J}_s^e$. The situation corresponds entirely to the situation from Fig. B-1, and the same reciprocity-theorem rule may be applied here.

Since we are interested in the TEM wave only, the z-components of the both electric and magnetic fields are zero. However, since both the electric and magnetic current sources are present, (B-5) has to be supplemented to include the magnetic current. Also, since the equivalent current is not distributed over the volume, but only over the surface of the aperture, the rule for computing C^+ becomes

$$2C^+_{TEM} = \int_{aperture} (\vec{h}_{TEM} \cdot \vec{J}^m_s - \vec{e}_{TEM} \cdot \vec{J}^e_s)\, e^{jkz} dS \quad , \qquad \text{(B-6)}$$

where the subscripts s denote surface currents in Amperes per meter. This formula will be now used to find the magnitudes C^-_{TEM} and C^+_{TEM} of the TEM waves induced by the sources $\vec{J}^m_s$ and $\vec{J}^e_s$ as shown in Fig. B-3. The electric and magnetic fields of the TEM wave on a circular wire above the ground plane have been derived in Appendix A. They are as follows

$$\vec{E}_{TEM} = E_x \vec{a}_x + E_y \vec{a}_y \quad , \qquad \text{(B-7)}$$

$$\vec{H}_{TEM} = -\frac{Ey}{\eta}\vec{a}_x + \frac{Ex}{\eta}\vec{a}_y . \qquad \text{(B-8)}$$

The normalized fields $\vec{e}_{TEM}$ and $\vec{h}_{TEM}$ of the TEM wave propagating in positive z direction are to be defined in the following way:

$$\vec{E}_{TEM} = \frac{V_o^+}{\sqrt{Z_o}} \vec{e}_{TEM}(x,y) e^{-jkz} \qquad \text{(B-9)}$$

$$\vec{H}_{TEM} = \frac{V_o^+}{\sqrt{Z_o}} \vec{h}_{TEM}(x,y) e^{-jkz} \qquad \text{(B-10)}$$

Then, the total power transmitted by the TEM propagating wave is

$$P_{TEM} = \tfrac{1}{2}\mathrm{Re} \int_{\text{cross section}} (\vec{E}_{TEM} \times \vec{H}^{*}_{TEM}) \cdot d\vec{S}$$

$$= \frac{|V_o^+|^2}{2Z_o} \int_{\text{cross section}} (\vec{e}_{TEM} \times \vec{h}_{TEM}) \cdot d\vec{S}$$

$$= \frac{|V_o^+|^2}{2Z_o} \qquad \text{(B-11)}$$

because of (B-3). Obviously, the result is consistent with the circuit theory. For the traveling wave, the total voltage V_o is equal to the incident-wave voltage V_o^+. Thus, the normalized modal fields are found by comparing (B-9) and (B-10) with (A-8), (A-9), and (A-13):

$$\vec{e}_{TEM} = \vec{a}_x \left(\frac{2\eta h}{\pi\sqrt{Z_o}} \cdot \frac{xy}{[x^2+(y-h)^2][x^2+(y+h)^2]}\right)$$

$$-\vec{a}_y \left(\frac{\eta h}{\pi\sqrt{Z_o}} \cdot \frac{h^2+x^2-y^2}{[x^2+(y-h)^2][x^2+(y+h)^2]}\right) \quad , \qquad \text{(B-12)}$$

$$\vec{h}_{TEM} = \frac{1}{\eta}\vec{a}_z \times \vec{e}_{TEM} \quad . \qquad \text{(B-13)}$$

The modal fields are now explicitely known. They can be substituted in (B-6) in order to compute the wave amplitude C_{TEM}^+ for any aperture for which the equivalent surface electric and magnetic currents $\vec{J}_s^e$ and $\vec{J}_s^m$ are known.

The computation is especially simple when the source currents take the form of delta functions:

$$\vec{J}_s^m = \vec{m}_a \; \delta(x-x_o) \; \delta(z-z_o), \qquad \text{(B-14)}$$

$$\vec{J}_s^e = \vec{p}_a \; \delta(x-x_d) \; \delta(z-z_o), \qquad \text{(B-15)}$$

where $\vec{m}_a$ and $\vec{p}_a$ are the magnetic and electric dipole moments of the aperture (in Volt-meters and Ampere-meters). When (B-14) and (B-15) are substituted in (B-6), the result is

$$C^+_{TEM} = \tfrac{1}{2}[h_{xTEM}(x_o,0)\ m_{xa} - e_{yTEM}(x_o,0)\ p_{ya}]e^{jkz_o} \quad , \qquad \text{(B-16)}$$

since h_{xTEM} and e_{yTEM} are the only two non-zero field components (see Fig. B-5) at the surface of the ground plane (y=0).

C^+_{TEM} has the meaning of the usual scattering-parameter amplitude:

$$C^+_{TEM} = \frac{V^+_o}{\sqrt{Z_o}} \quad , \qquad \text{(B-17)}$$

so that the total power carried by the TEM wave is

$$P_{TEM} = \tfrac{1}{2}\mathrm{Re} \int_{\text{cross section}} (\vec{E}_{TEM} \times \vec{H}^*_{TEM}) \cdot d\vec{S} = \tfrac{1}{2} |C^+_{TEM}|^2 . \qquad \text{(B-18)}$$

The dimensions of C^+_{TEM} are $\text{Watts}^{\frac{1}{2}}$.

In order to compute the amplitude C^-_{TEM} of the wave traveling in the negative z direction, the reaction is to be taken with a unit-amplitude TEM wave propagating in the positive z direction. Also, one has to note that for the wave propagating in negative z direction the $\vec{e}_{TEM}$ remains such as in (B-12), but the $\vec{h}_{TEM}$ has the sign opposite of (B-13). With these changes in mind, the formula (B-6) becomes

$$2C^-_{TEM} = \int_{\text{aperture}} (-\vec{h}_{TEM} \cdot \vec{J}^m_s - \vec{e}_{TEM} \cdot \vec{J}^e_s) e^{-jkz} dS. \qquad \text{(B-19)}$$

When the sources are delta functions (B-14) and (B-15), the amplitude C^-_{TEM} of the wave traveling in the negative z direction becomes

$$C^-_{TEM} = -\tfrac{1}{2}[h_{xTEM}(x_o,0)\ m_{xa} + e_{yTEM}(x_o,0)\ p_{ya}]e^{-jkz_o} \quad . \qquad \text{(B-20)}$$

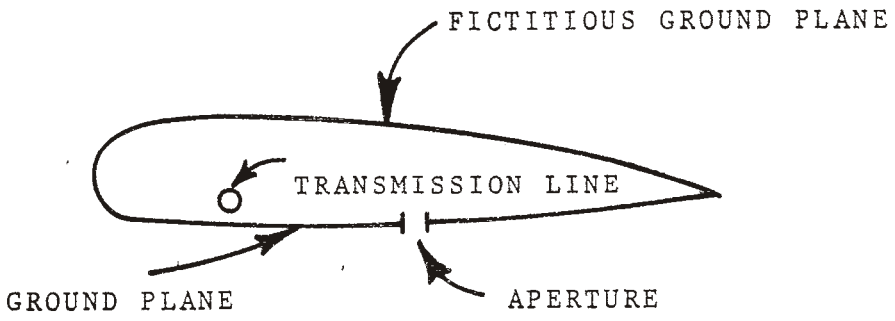

Fig. B-4. Airplane wing is a justification for the upper ground plane.

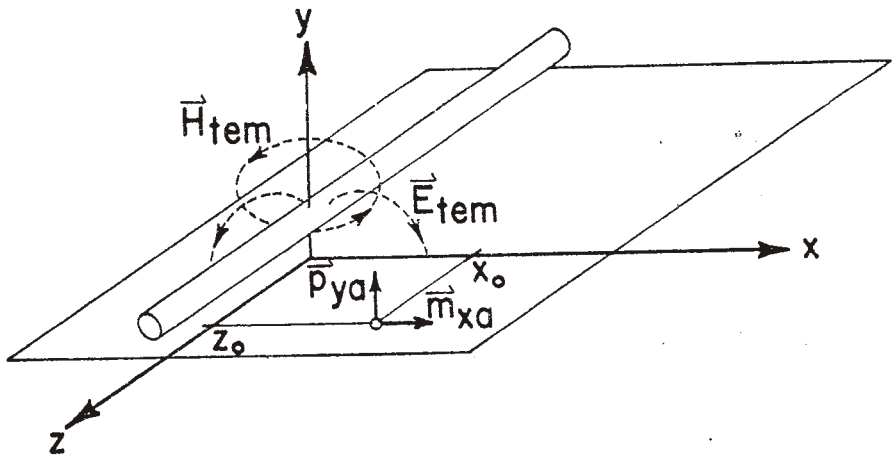

Fig. B-5. Orientation of electric and magnetic fields on a TEM transmission line.

APPENDIX C

Coupling Coefficients for TEM Mode Excited by Localized Current Sources. (Mode Matching Method)

In Fig. C-1, an infinitely long transmission line is excited by a localized distribution of current sources. Sheath S has a finite size, it is situated in the x-y plane, and it contains surface electric currents $\vec{J}_s^e$ (in amperes/meter) and surface magnetic currents $\vec{J}_s^m$ (in volts/meter). Assuming that $\vec{J}_s^e$ and $\vec{J}_s^m$ are known functions of position, we want to compute the voltages and currents on the transmission line (denoted by V_{10}, V_{20}, I_{10}, and I_{20} in Fig. C-1).

Total electric and magnetic fields on a transmission line may be represented as a sum over all propagating and nonpropagating modes. It will be assumed that only a TEM mode is propagating at frequency of interest. The electromagnetic field at z = 0+ is, therefore

$$\vec{E}_1 = \frac{V_{1o}}{\sqrt{Z_o}} \vec{e}_{TEM} + \sum_n \frac{V_{1n}}{\sqrt{Z_n}} \vec{e}_n \quad , \qquad (C\text{-}1)$$

$$\vec{H}_1 = I_{1o}\sqrt{Z_o}\, \vec{h}_{TEM} + \sum_n \vec{I}_{1n}\sqrt{Z_n}\, \vec{h}_n \quad . \qquad (C\text{-}2)$$

On the other side of the boundary, at z = 0- the field is

$$\vec{E}_2 = \frac{V_{20}}{\sqrt{Z_o}} \vec{e}_{TEM} + \sum_n \frac{V_{2n}}{\sqrt{Z_n}} \vec{e}_n \quad , \qquad (C\text{-}3)$$

$$\vec{H}_2 = -I_{20}\sqrt{Z_o}\, \vec{h}_{TEM} - \sum_n I_{2n}\sqrt{Z_n}\, \vec{h}_n \quad , \qquad (C\text{-}4)$$

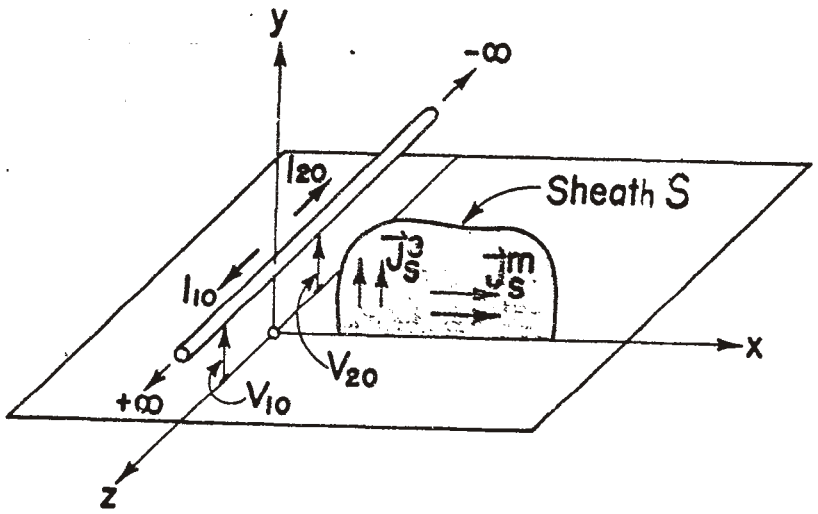

Fig. C-1. Excitation of the transmission line by a sheath of electric and magnetic currents.

the negative sign coming from the fact that the direction of I_{20} is along the negative z axis, as in Fig. C-1. The further discussion is considerably simplified if we define the abstract scalar product of two vectors $\vec{A}(x,y)$ and $\vec{B}(x,y)$ as follows

$$< \vec{A} , \vec{B} > = \int_{x=-\infty}^{\infty} \int_{y=0}^{\infty} (\vec{A} \times \vec{B}^*) \cdot \vec{a}_z \, dxdy \quad . \tag{C-5}$$

If $\vec{A}$ or $\vec{B}$ have non-zero values only within the limited range of x or y, the integration will be naturally restricted to this range only. Note that if $\vec{A} = \vec{E}$ and $\vec{B} = \vec{H}$, this scalar product has a physical meaning of the Poynting vector flux. For complex values of $\vec{E}$ and $\vec{H}$ (peak values), one half of the real part of the scalar product represents the average power flux along the transmission line. In Appendix B, the modal fields $\vec{e}_{TEM}$ and $\vec{h}_{TEM}$ were defined as real functions normalized in the following way:

$$< \vec{e}_{TEM} , \vec{h}_{TEM} > = 1 \quad . \tag{C-6}$$

It will be assumed that all the other modes are evanescent, and orthogonal to the TEM modes:

$$\text{Re} < \vec{e}_n , \vec{h}_n > = 0 \quad ; \tag{C-7}$$

$$\text{Re} < \vec{e}_n , \vec{h}_{TEM} > = \text{Re} < \vec{h}_n , \vec{e}_{TEM} > = 0. \tag{C-8}$$

Along the sheath S containing the surface currents $\vec{J}_s^m$ and $\vec{J}_s^e$, the boundary conditions are [C.1]:

$$\vec{a}_z \times (\vec{H}_1 - \vec{H}_2) = \vec{J}_s^e \quad , \tag{C-9}$$

$$\vec{a}_z \times (\vec{E}_2 - \vec{E}_1) = \vec{J}_s^m \quad . \tag{C-10}$$

The electromagnetic fields will be next expressed in terms of expansions (C-1) through (C-4) and the equality of both sides

of the equation (C-9) will be enforced in terms of the abstract scalar product defined earlier. Thus, the scalar product of (C-9) with $\vec{h}_{TEM}$ gives

$$< \vec{a}_z \times (\vec{H}_1 - \vec{H}_2) , \vec{h}_{TEM} > = < \vec{J}_s^e , \vec{h}_{TEM} > . \qquad (C-11)$$

Assuming that only TEM is propagating and that all the modes are orthogonal, only the TEM-term in the expansions for $\vec{H}_1$ and $\vec{H}_2$ contributes to the real part of the above scalar product. Using (C-2) and (C-4) gives

$$\sqrt{Z_o} <\vec{a}_z \times (I_{10} + I_{20}) \vec{h}_{TEM} , \vec{h}_{TEM} > = < \vec{J}_s^e , \vec{h}_{TEM}> . \qquad (C-12)$$

Furthermore, from (B-13) the magnetic field of a TEM wave can be expressed in terms of the electric field as follows:

$$\vec{h}_{TEM} = \frac{1}{\eta} \vec{a}_z \times \vec{e}_{TEM} . \qquad (C-13)$$

Since $\vec{e}_{TEM}$ is perpendicular to $\vec{a}_z$, (C-12) and (C-13) give the following result

$$- \frac{\sqrt{Z_o}}{\eta} (I_{10} + I_{20}) = \int (J_{xs}^e \, h_{yTEM} - J_{ys}^e \, h_{xTEM}) dxdy . \qquad (C-14)$$

In an analogous way, a scalar product is formed of (C-10) with $\vec{e}_{TEM}$ and the following result is obtained

$$\frac{\eta}{\sqrt{Z_o}} (V_{20} - V_{10}) = \int (J_{xs}^m \, e_{yTEM} - J_{ys}^m \, e_{xTEM}) dxdy . \qquad (C-15)$$

The integrations involved in (C-14) and (C-15) are greatly simplified when the electric and magnetic currents take the form of delta functions (Appendix D), like in the case of a small aperture:

$$\vec{J}_s^e (x,y,0) = \vec{p}_a \, \delta(x-x_o)\delta(y) , \qquad (C-16)$$

$$J_s^m (x,y,0) = \vec{m}_a \, \delta(x-x_o)\delta(y) \quad . \qquad (C-17)$$

Furthermore, on the surface of the metal, $\vec{e}_{TEM}$ has only the y component and $\vec{h}_{TEM}$ has only the x component. Therefore, for small aperture the induced voltages and currents are

$$I_{10} + I_{20} = \Delta I = \frac{-1}{\sqrt{Z_o}} p_{ya} \, e_{yTEM} (x_o,0) \qquad (C-18)$$

$$V_{20} - V_{10} = \Delta V = -\sqrt{Z_o} \, m_{xa} \, h_{xTEM} (x_o,0) \qquad (C-19)$$

The values of ΔI and ΔV depend only on the corresponding components of the electric and magnetic dipole moments and on the dimensions of the cross section of the transmission line. ΔI and ΔV do not depend on the load conditions at the transmission line terminals. Therefore, an equivalent circuit for the voltages and currents on the transmission line can be drawn as shown in Fig. C-2.

The traveling wave amplitudes V_1^- and V_2^+ on the transmission line may be computed as follows. From the Ohm's law

$$\frac{V_{20}}{I_{20}} = \frac{V_{10}}{I_{10}} = Z_o \qquad (C-20)$$

Thus we can eliminate I_{10} and I_{20} in (C-17) and (C-18) and obtain

$$V_1^- = V_{10} = \frac{1}{2} (Z_o \Delta I - \Delta V) \quad , \qquad (C-21)$$

$$V_2^+ = V_{20} = \frac{1}{2} (Z_o \Delta I + \Delta V) \quad , \qquad (C-22)$$

since on an infinite transmission line, the total voltage consists of the outgoing voltage wave only. By normalizing traveling waves as in Appendix B:

$$C^+ = \frac{V_2^+}{\sqrt{Z_o}} \quad , \quad C^- = \frac{V_1^-}{\sqrt{Z_o}} \quad , \qquad (C-23)$$

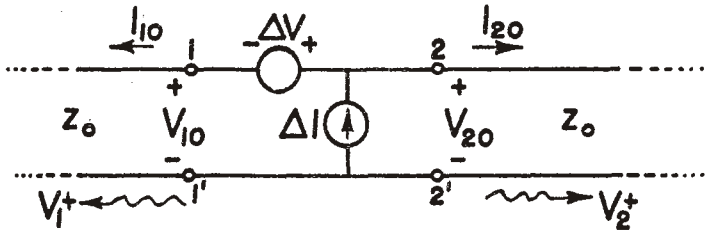

Fig. C-2. Equivalent circuit for the transmission line.

one obtains the outgoing wave amplitudes as follows:

$$C^{+} = \frac{1}{2} \left(m_{xa} \, h_{xTEM} - p_{ya} \, e_{yTEM} \right) \quad , \tag{C-24}$$

$$C^{-} = \frac{-1}{2} \left(m_{xa} \, h_{xTEM} + p_{ya} \, e_{yTEM} \right) \quad . \tag{C-25}$$

The results are in agreement with (B-16) and (B-20). Therefore, the mode matching method and the reciprocity theorem method both lead to the same result.

APPENDIX D

Aperture Representation by a Pair of Dipoles

Assume that the distribution of the EM field in a given aperture is a known function. To compute the scattered field in the "inside" region one needs to know only the tangential electric field $\vec{E}_t$ over the aperture (Fig. D-1a). It is convenient to close the aperture and place magnetic surface current $\vec{J}_s^m$ over the area which was previously occupied by aperture:

$$\vec{J}_s^m = \vec{E}_t \times \vec{n} \qquad \text{(D-1)}$$

as shown in Fig. D-1b. Now, the scattered field anywhere in the "inside" region may be computed from the known value of the source $\vec{J}_s^m$, resting on the surface of a metal plane without aperture.

Computation of the field $\vec{E}_a$, scattered by the aperture, is conveniently performed by the use of the reciprocity theorem. In Fig. D-2, the origin of coordinates is located in the region over which there exists a source current $\vec{J}_s^m$. At the position $\vec{r}_o$, the field produced by $\vec{J}_s^m$ is $\vec{E}_a(\vec{r}_o)$. To test this field, a unit-magnitude electric dipole $\vec{p}$ of suitable orientation is located at $\vec{r}_o$:

$$\vec{p} = \vec{a}_p \, \delta(\vec{r}-\vec{r}_o) \qquad \text{(D-2)}$$

where $\vec{a}_p$ is a unit vector specifying the orientation of the testing dipole $\vec{p}$, and $\delta(\vec{r}-\vec{r}_o)$ is a delta function having the property

$$\int_V f(\vec{r})\,\delta(\vec{r}-\vec{r}_o)\,dV = f(\vec{r}_o) \quad . \qquad \text{(D-3)}$$

The reciprocity theorem can be formulated in various ways, as it is discussed in detail in the Mathematics Note 33, ref [D.1]. For the situation shown in Fig. D-2, the following form of the

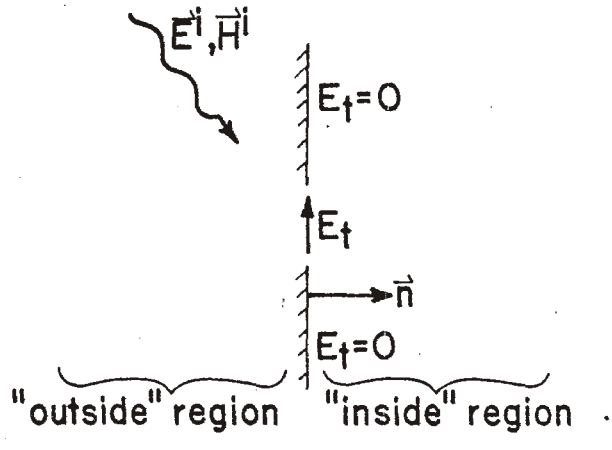

Fig. D-1a.
Aperture in the screen.

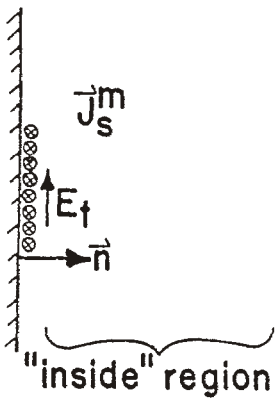

Fig. D-1b.
Aperture replaced by a surface magnetic current $\vec{J}_s^m$.

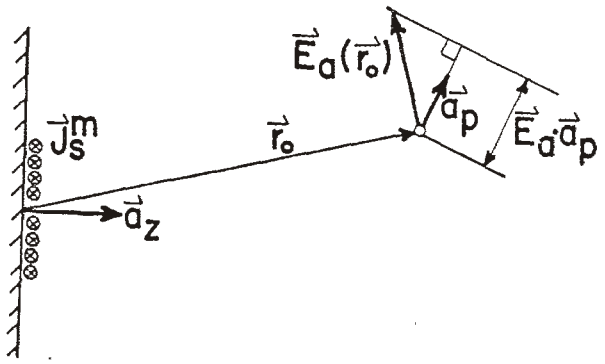

Fig. D-2. Evaluation of the p-component of the "inside" electric field by the use of reciprocity theorem.

reciprocity theorem is used [D.2]:

$$\vec{a}_p \cdot \vec{E}_a(\vec{r}_o) = \int_V (\vec{J}^e \cdot \vec{E}_b - \vec{J}^m \cdot \vec{H}_b)\, dV \quad . \qquad \text{(D-4)}$$

$\vec{E}_b$ and $\vec{H}_b$ are the fields produced by the source $\vec{p}$ and evaluated at the surface of the aperture when the aperture is closed by a perfectly conducting lid. When the practical computation is performed, this field will look like a pair of two waves, one incident in the direction from source $\vec{p}$ toward the center of coordinates, and the other being reflected from the metal surface. Therefore, the magnetic field tangential to the metal surface and the electric field normal to the metal surface will have magnitudes equal to twice the magnitudes of the corresponding incident fields.

In the case of an aperture, the integration indicated in (D-4) is performed over the surface instead of over the volume, so that one obtains

$$\vec{a}_p \cdot \vec{E}_a(\vec{r}_o) = \int_S (\vec{J}_s^e \cdot \vec{E}_b - \vec{J}_s^m \cdot \vec{H}_b)\, dS \quad . \qquad \text{(D-5)}$$

$\vec{J}_s^e$ and $\vec{J}_s^m$ are surface electric and magnetic currents, which are the sources of the field scattered by the aperture. In the case considered here, $\vec{J}_s^m$ is given by (D-1), and $\vec{J}_s^e = 0$. Therefore, in order to compute the p-component of the field $\vec{E}_a$ scattered by the aperture, one needs to know only the behavior of the tangential component of the magnetic field $\vec{H}_b$ over the region where there was an aperture (but it is not there any more.)

In order to facilitate further discussion, the rectangular coordinates of the aperture region will be denoted by x and y, as shown in Fig. D-3a. Note that the x-axis has been chosen to coincide with the orientation of $\vec{H}_b$. The corresponding electric field $\vec{E}_b$ follows from Maxwell's equation:

$$\nabla \times \vec{H}_b = j\omega\varepsilon\vec{E}_b \qquad \text{(D-6)}$$

Since $\vec{H}_b$ has only the x-component, (D-6) gives

$$\frac{\partial H_{bx}}{\partial y} = -j\omega\varepsilon E_{bz} \quad . \tag{D-7}$$

Field $\vec{H}_b$, $\vec{E}_b$ is produced by a dipole $\vec{p}$ at distance $|\vec{r}_o|$ away from the aperture. If the aperture dimensions are smaller than $|\vec{r}_o|$, then the field variations over the aperture region will be smooth and slight. It is legitimate to expand the field in a Taylor series and retain only the first three terms:

$$H_{bx}(x,y) \approx H_{bx}(0,0) + \frac{\partial H_{bx}(0,0)}{\partial x}x + \frac{\partial H_{bx}(0,0)}{\partial y}y \quad . \tag{D-8}$$

When the lateral displacement of the hole in Fig. 2-1 is small,

$$x_o << d \quad , \tag{D-9}$$

the second term in (D-8) vanishes:

$$\frac{\partial H_{bx}(0,0)}{\partial x} \approx 0 \quad . \tag{D-10}$$

However, this is not true when $x_o \geq d$, and the second term should be taken into account by including it in the quadrupole contribution, as done in [D-3]. In the present report only the dipole contribution is considered, so that the assumption (D-10) will be made even when (D-9) is not true. The third term in (D-8) can be related to E_{bz} through (D-7), so that the expansion for H_{bx} becomes:

$$H_{bx}(x,y) \approx H_{bx}(0,0) - j\omega\varepsilon E_{bz}(0,0)y \quad . \tag{D-11}$$

Then, the reaction integral in (D-5) becomes

$$\vec{a}_p \cdot \vec{E}_a(\vec{r}_o) = -\int_s \vec{J}_s^m \cdot \vec{H}_b \, dS$$

$$\approx -\iint [H_{bx}(0,0) - j\omega\varepsilon E_{bz}(0,0)y] J_{sx}^m(x,y)\,dxdy \quad . \tag{D-12}$$

Taking constants out of the integration one obtains

$$\vec{a}_p \cdot \vec{E}_a(\vec{r}_o) = -H_{bx}(0,0)a_o + j\omega\varepsilon E_{bz}(0,0)a_1 \quad , \tag{D-13}$$

where a_o and a_1 represent the zeroth and the first moment of the J^m_{sx} function as follows

$$a_o = \iint J^m_{sx}(x,y)dxdy \quad , \tag{D-14}$$

$$a_1 = \iint yJ^m_{sx}(x,y)dxdy \quad . \tag{D-15}$$

Comparing the approximate equation (D-13) with the exact equation (D-5) one can come to the following interpretation. The aperture is producing such a far field $\vec{E}_a(\vec{r}_o)$, as if the source consisted of two point sources: one magnetic surface current

$$\vec{J}^m_s = \vec{m}_a \, \delta(x)\delta(y) \quad , \tag{D-16}$$

and one electric surface current

$$\vec{J}^e_s = \vec{p}_a \, \delta(x)\delta(y) \quad . \tag{D-17}$$

The magnetic dipole moment is

$$\vec{m}_a = \vec{a}_x a_o = \vec{a}_x \iint \vec{J}^m_{sx}(x,y)dxdy \quad , \tag{D-18}$$

and the electric dipole moment is

$$\vec{p}_a = \vec{a}_z j\omega\varepsilon a_1 = \vec{a}_z j\omega\varepsilon \iint yJ^m_{sx}(x,y)dxdy \quad . \tag{D-19}$$

The situation is depicted in Fig. D-3b. Consequently, for purposes of calculation of the field scattered by the aperture at distances considerably larger than the aperture size, the aperture may be represented by a pair of electric and magnetic dipoles (= point sources). Indeed if one substitutes (16) and (17) into (5), one obtains the same result (13) as from the Taylor's expansion of

the fields over the aperture. The equivalence is obviously good only in a low frequency limit, when the aperture is small in comparison with the wavelength so that the first three terms in Taylor's expansion (D- 8) offer all the needed details of the field variation. It is possible to continue the expansion to quadrupoles, as done by Collin [D.3], at the expense of considerable loss in simplicity.

As an example, consider the small circular aperture. Jackson [D.4] gives the expression for the tangential field in the plane of the opening as follows (SI units):

$$\vec{E}_{tan} = E_o \frac{\vec{\rho}}{\pi\sqrt{a^2-\rho^2}} + \frac{2j\omega\mu}{\pi} (\vec{a}_z \times \vec{H}_o) \sqrt{a^2-\rho^2} \quad , \qquad (D\text{-}20)$$

where E_o is the z-component of the external electric field in the absence of the hole and $\vec{H}_o$ is the tangential external magnetic field in the absence of the hole. In EMP terminology, these are the short-circuit normal electric and tangential magnetic fields, in the "outside" region. $\vec{\rho}$ is the radius vector of the circular aperture (see Fig. D-4). The vector product $(\vec{a}_z \times \vec{H}_o)$ is a vector laying in the aperture plane, its magnitude equal to H_o and its direction defined by a unit vector $\vec{a}_t$ (see Fig. D-4). Note that $\vec{a}_t$ is perpendicular to the actual short-circuit tangential field $\vec{H}_o$. Using the unit vectors $\vec{a}_t$ and $\vec{a}_\rho$, (D-20) can be rewritten as

$$\vec{E}_{tan} = \vec{a}_\rho \frac{E_o\rho}{\pi\sqrt{a^2-\rho^2}} + \vec{a}_t \frac{j2\omega\mu H_o}{\pi} \sqrt{a^2-\rho^2} \quad . \qquad (D\text{-}21)$$

According to Fig. D-4 one can express everything in rectangular coordinates x and y as follows:

$$\rho^2 = x^2 + y^2 \quad , \qquad (D\text{-}22)$$

$$\vec{a}_\rho = \vec{a}_x \cos\phi + \vec{a}_y \sin\phi \quad , \qquad (D\text{-}23)$$

$$\vec{a}_t = \vec{a}_x \cos\alpha + \vec{a}_y \sin\alpha \quad . \qquad (D\text{-}24)$$

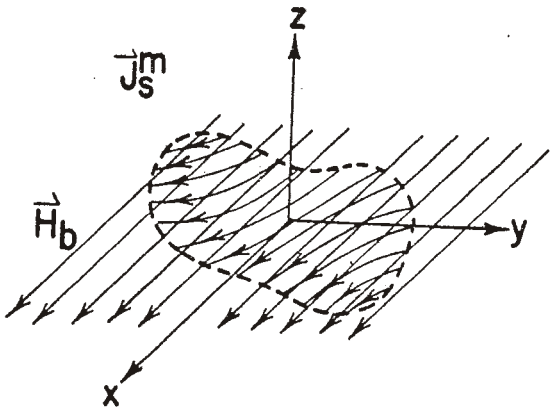

Fig. D-3a.
Interaction of the magnetic surface current $\vec{J}_s^m$ with slowly varying field $\vec{H}_b$.

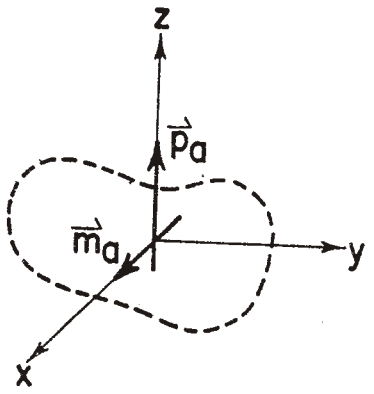

Fig. D-3b.
$\vec{J}_s^m$ is replaced by a pair of moments.

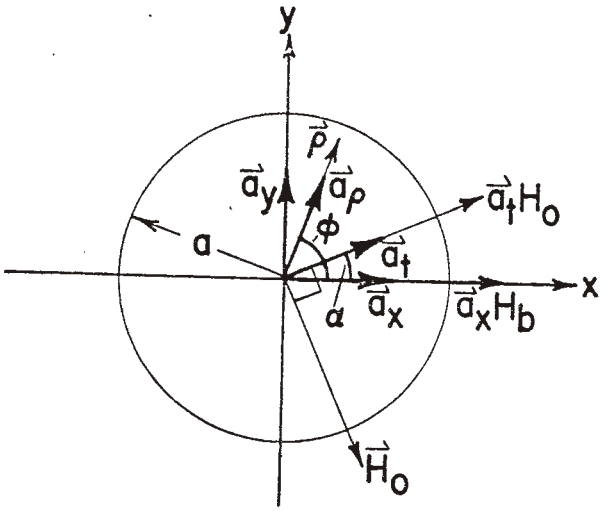

Fig. D-4. Computation of dipole moments of a circular aperture.

The $\vec{E}_{tan}$ from (D-21) will be replaced by a solid metal wall plus an equivalent magnetic surface current, such as in Fig. D-1b. From (D-1), this equivalent magnetic surface current is

$$\vec{J}_s^m = \vec{E}_{tan} \times \vec{a}_z \qquad \text{(D-25)}$$

Using (D-22) to(D-24) one obtains the x-component of $\vec{J}_s^m$

$$J_{sx}^m = \frac{E_o \rho \sin\phi}{\pi\sqrt{a^2-\rho^2}} + j\frac{2}{\pi}\,\omega\mu H_o \sin\alpha\,\sqrt{a^2-\rho^2} \quad . \qquad \text{(D-26)}$$

The computation of equivalent aperture moments $\vec{m}_a$ and $\vec{p}_a$ is now performed according to (D-18) and (D-19). For the circular aperture, it is convenient to integrate in polar, instead of rectangular, coordinates

$$\vec{m}_a = \vec{a}_x \int_{\rho=0}^{a} \int_{\phi=0}^{2\pi} \left[\frac{E_o \rho^2 \sin\phi}{\pi\sqrt{a^2-\rho^2}} + j\frac{2}{\pi}\,\omega\mu H_o \rho \sin\alpha\,\sqrt{a^2-\rho^2}\right] d\rho\, d\phi \quad . \qquad \text{(D-27)}$$

The first term vanishes and the result of integration is

$$\vec{m}_a = \vec{a}_x j\frac{4}{3}\,\omega\mu a^3 H_o \sin\alpha \quad . \qquad \text{(D-28)}$$

Similarly, the equivalent electric dipole moment of the aperture is found from (19) and (26)

$$\vec{p}_a = \vec{a}_z j\frac{2}{3}\,\omega\varepsilon a^3 E_o \quad . \qquad \text{(D-29)}$$

References

[1] C. E. Baum, "General Principles for the Design of Atlas I and II, Part V: Some Approximate Figures of Merit for Comparing the Waveforms Launched by Imperfect Pulser Arrays onto TEM Transmission Lines", Interaction Note 148, May 1972.

[2] C. E. Baum, K. S. H. Lee, "Application of Modal Analysis to Braided-Shield Cables", Interaction Note 132, January 1973.

[3] C. E. Baum, "Some Characteristics of Electric and Magnetic Dipole Antennas for Radiating Transient Pulses", Sensor and Simulation Note 125, January 1971, p. 16.

[4] S. A. Schelkunoff, Electromagnetic Waves, Princeton: Van Nostrand, 1943, p. 129.

[5] R. F. Harrington, Time-Harmonic Electromagnetic Fields, New York: McGraw-Hill, 1961, p. 78.

[6] W. L. Weeks, Electromagnetic Theory for Engineering Applications, New York: Wiley, 1964, p. 310.

[7] S. A. Schelkunoff, Electromagnetic Waves, Princeton: Van Nostrand, 1943, p. 162.

[8] R. F. Harrington, Time-Harmonic Electromagnetic Fields, New York: McGraw-Hill, 1961, p. 100.

[9] W. L. Weeks, Electromagnetic Theory for Engineering Applications, New York: Wiley, 1964, p. 565.

[A.1] E. Weber, Electromagnetic Theory, New York: Dover, 1965, p. 116-119.

[A.2] R. E. Collin, Field Theory of Guided Waves, New York: McGraw-Hill, 1960, p. 68.

[A.3] E. Della Torre, C. V. Longo, The Electromagnetic Field, Boston: Allyn and Bacon, 1969, p. 202.

[B.1] R. E. Collin, Foundations for Microwave Engineering, New York: McGraw-Hill, 1966, p. 185.

[C.1] R. F. Harrington, Time-Harmonic Electromagnetic Fields, New York: McGraw-Hill, 1961, p. 34.

[D.1] C. E. Baum, "Electromagnetic Reciprocity and Energy Theorem for Free Space Including Sources Generalized to Numerous Theorems, to Combined Fields, and to Complex Frequency Domain, Mathematics Note 33, December 1973.

[D.2] W. L. Weeks, Electromagnetic Theory for Engineering Applications, New York: Wiley, 1964, p. 323.

[D.3] R. E. Collin, Field Theory of Guided Waves, New York: McGraw-Hill, 1960, p. 292.

[D.4] J. D. Jackson, Classical Electrodynamics, New York: Wiley, 1962, p. 298.